INFORMATION THEORETICAL PERFORMANCE ANALYSIS AND OPTIMIZATION OF UNDERWATER ACOUSTIC COMMUNICATION SYSTEMS

A Thesis

by

Hatef Nouri

Submitted to the
Graduate School of Sciences and Engineering
In Partial Fulfillment of the Requirements for
the Degree of

Master of Science

in the
Department of Electrical and Electronics Engineering

Özyeğin University
August 2013

INFORMATION THEORETICAL PERFORMANCE ANALYSIS AND OPTIMIZATION OF UNDERWATER ACOUSTIC COMMUNICATION SYSTEMS

Approved by:

Professor Murat Uysal, Advisor
Department of Electrical and Electronics Engineering
Özyeğin University

Professor Ali Özer Ercan
Department of Electrical and Electronics Engineering
Özyeğin University

Professor Hacı İlhan
Department of Electronics and Communications Engineering
Yıldız Teknik University

Date Approved: 19 August 2013

To My dear parents

ABSTRACT

Underwater wireless communication is a rapidly growing field of research and engineering as its applications, which were once exclusively military, are extending into commercial fields. The need for underwater wireless communications exists in a wide range of applications including offshore oil field exploration/monitoring, oceanographic data collection, maritime archaeology, seismic observation, environmental monitoring, disaster preventing, port and border security among many others. Although capacity calculations for terrestrial radio-frequency channels have been extensively studied, the literature on the capacity of underwater acoustic (UWA) channels is sporadic with many remaining open questions. Aiming to fill research gaps in this growing field, this thesis makes several contributions to the information theoretical performance analysis of point-to-point and relay-assisted UWA systems. A single-carrier communication architecture and sparse Rician frequency-selective UWA channel with intersymbol interference (ISI) is considered in our work. We assume non-white Gaussian distribution to model the ambient noise and consider Francois-Garrison path loss formula to take into account the effects of environmental parameters such as temperature, salinity, pressure as well as system parameters such as distance and frequency. We develop an equivalent channel model for UWA channel with ISI under consideration and show that the capacity of the equivalent channel converges to that of the operating channel in the limit of infinite block length. Using these results, we first obtain a capacity expression for the UWA channel and demonstrate the dependency on channel parameters such as the number and location of significant taps and power delay profile, and environmental parameters such as temperature, salinity, and pressure. Then, we use this expression to determine

the optimal carrier frequency, input signaling, and bandwidth. A closed-form formula for the optimum carrier frequency is further obtained. In the second part of the thesis, we extend our results to cooperative UWA systems and obtain achievable rates of single-carrier cooperative UWA systems with orthogonal decode-and-forward (DF) relaying. We take into account the effect of relay geometry in the derivations of achievable rates, and use the derived expressions to optimize location of the relay.

ÖZETÇE

Kablosuz sualtı haberleşme alanındaki araştırma ve mühendislik faaliyetleri hızla gelişmektedir. Bir zamanlar sadece askeri uygulamalar söz konusu iken, günümüzde sivil amaçlı uygulamaları da ortaya çıkmaktadır. Sualtı kablosuz haberleşmenin kullanıldığı uygulamalara örnek olarak petrol arama/izleme, oşinografik bilgi toplama, deniz arkeolojisi, sismik gözlem, çevresel gözlem, afet önleme, liman ve sınır güvenliği sayılabilir. Karasal radyo kanal kapasitesi üzerine kapsamlı hesaplama çalışmaları bulunmasına rağmen, sualtı akustik kanal kapasitesi üzerindeki çalışmaların sayısı azdır; dolayısıyla bu alanda açık birçok araştırma problemi bulunmaktadır. Bu tezde, gelişmekte olan bu alandaki mevcut araştırma boşluğunu doldurmak amacıyla, noktadan noktaya ve röle destekli sualtı akustik haberleşme sistemlerinin bilgi kuramı perspektifinden başarım analizleri yapılmıştır. Çalışmada tek taşıyıcılı bir system mimarisi ele alınmış ve seyrek Rician sönümleme ile simgelerarası girişime maruz kaldığı varsayılmıştır. Kanaldaki gürültüyü modellemek için ise, beyaz olmayan Gaussian dağılımı kullanılmış; sıcaklık, tuzluluk oranı, basınç, mesafe ve frekans gibi çevresel parametreleri de kanal modeline dahil etmek adına, Francois-Garrison yol kaybı formülü kullanılmıştır.

Tezin ilk kısmında, sualtı akustik kanal için eşdeğer bir kanal modeli geliştirilmiş ve bilgi çerceve genişliği sonsuza gittiğinde kanal kapasitesi ifadesi elde edilmiştir. Bu ifadenin ışığında, kanal kademe yer ve sayısı, güç gecikme profili gibi kanal parametreleri ile sıcaklık, tuzluluk oranı ve basınç gibi çevresel etkenlerin kanal kapasitesine etkisi ortaya konmuştur. Ardından, kanal kapasitesini eniyileyecek şekilde optimum taşıyıcı frekansı, giriş sinyali ve bant genişliği tesbit edilmiştir. Optimum taşıyıcı frekansı için analitik bir ifade çıkarımı da yapılmıştır. Tezin ikinci kısmında ise,

tek taşıyıcılı işbirlikli sualtı haberleşme sistemlerinde çöz-ve-ilet röleleme varsayımı altında erişilebilir veri hızı çıkartılmıştır. Hesaplamalarımızda röle noktalarının yerleri de göz önünde bulundurulmuş ve başarımı eniyileyecek şekilde röle yerleri tesbit edilmiştir.

ACKNOWLEDGEMENTS

I would like to express my special appreciation and thanks to my supervisor, Professor Murat Uysal, for his insightful suggestions, excellent guidance and motivations. This thesis would have not been possible without his consistence support throughout the course of my M.Sc. studies. Your complete dedication to your research is certainly something I admire, and your constant drive to ensure your work is relevant to scientists around the world is truly impressive. I hope I am able to take some of that drive and commitment to excellence with me in my future endeavors.

I would like to express my appreciation to the members of my dissertation committee, Professors Ali Özer Ercan and Hacı İlhan, for taking the time to carefully read my thesis. Definitely, the guidance and support you have given me throughout my studies and this thesis would be a treasure for the rest of my life.

I would also like to thank all of my friends that have helped me in one way or another through the years. In particular, I'd like to thank Azadeh for friendship and support. You have helped me a lot through tough times and were always there with wisdom. I have been so lucky meeting you and thanks for being you. Thanks to Hamza and Mohammadreza, you have accompanied me from the start of my M.Sc. study and helped me a lot in my difficulties. Thanks for the memories and friendship.

I owe my deepest thanks to my family for all of their endless love and sincere encouragement. I am grateful to my parents who seem to believe in me no matter what I'm doing. With having you behind me I feel like I can do just about anything. Thanks to all of my friends for their support. I am truly grateful that so many people, who have no idea what I'm talking about, keep asking what I am up to. It's amazing how all of you can really keep a guy going.

TABLE OF CONTENTS

LIST OF TABLES

LIST OF FIGURES

CHAPTER I

INTRODUCTION

Underwater wireless communication is a rapidly growing field of research and engineering as the applications, which were once exclusively military, are extending into commercial fields. The need for underwater wireless communications exists in a wide range of applications including offshore oil field exploration/monitoring, oceanographic data collection, maritime archaeology, seismic observation, environmental monitoring, disaster preventing, port and border security among many others.

Underwater wireless communication can be achieved through radio, optical, or sound (acoustic) waves. The low frequency radio waves (30 Hz - 300 Hz) can propagate long distances through the sea water; however, require large antennas and high transmitter powers. Optical waves do not suffer so much from attenuation but are affected by scattering. In particular, those in the blue-green region, offer much higher throughput albeit over short distances (up to about 100 m). Among the three methods, acoustic transmission is the most practical and commonly employed method due to favorable propagation characteristics of sound waves in the underwater environments and therefore research efforts have mainly focused on acoustic communication.

The idea of transmitting information in underwater through acoustic waves, can be traced back to the time of Leonardo Da Vinci who could detect ships by listening on a long tube submerged under the sea [1]. In modern sense, one of the first underwater acoustic communication systems was developed during the Second World War for military purposes [2]. It used single-sideband suppressed carrier (SSB-SC) amplitude modulation and was capable of sending acoustic signals over distances of several kilometers within frequency range of 8-11 kHz.

Due to time variability and dispersive multipath propagation aspects of UWA channels, it was believed in the past that phase coherent modulation techniques such as phase shift keying (PSK) and quadrature amplitude modulation (QAM) can not be employed in UWA systems. Hence, in the 1980s, the UWA system designs were based on frequency shift keying (FSK) modulation. However, FSK suffers from bandwidth inefficiency and consequently low data rate. Following the increasing demands for high data rates in the 1990s, researchers started exploring the design of coherent acoustic modems [3]. Much research effort has particularly focused on the design of low-complexity equalization schemes, which is a key issue for underwater channels with large delay spreads. Particularly, sparse channel estimation/equalization and turbo equalization have been investigated by several research groups [4–7].

Emerging data-heavy underwater applications impose further requirements on acoustic modem design. To address such challenges, recent advances in terrestrial wireless radio-frequency systems have been succesfully applied to UWA communication. These include orthogonal frequency division multiplexing (OFDM) [8–10], multiple-input multiple-output (MIMO) communication techniques [11–14] and cooperative communication [15–17].

In UWA communcation system design, unique characteristics of UWA channel such as multipath fading, bandwidth limitations, and sparsity should be carefully taken into account. UWA channels suffer from time/frequency spreading and significant attenuation as a function of distance and frequency. In UWA channels, the transmitted signal is subject to multipath propagation and experiences frequency selectivity which causes intersymbol interference (ISI). In shallow water, reflections from bottom, surface, or any objects in the water, and in deep water, the effect of ray bending effect, cause multipath fading. Furthermore, in UWA channels, the path loss increases not only with range, but also with frequency which pose significant limitation on the available bandwidth [18]. Noise observed in the ocean exhibits

strong frequency dependence. Most of the ambient noise sources can be modeled by non-white correlated Gaussian noise [18].

For an efficient UWA communication system design, it is important to understand the fundamental performance limits imposed by the underwater channels. From an information theoretic point of view, the basic performance measure is the capacity of a channel which determines the maximum data rate that can be supported with an arbitrarily small error probability. Although capacity calculations for terrestrial radio-frequency (RF) channels have been extensively studied, the literature on the capacity of UWA channels is sporadic [19–21] with many remaining open questions. To the best of our knowledge, the capacity of UWA channel has been first studied by Kwon and Birdsall [22]. However, they oversimplify the UWA channel model ignoring the multipath fading effects and use a time-invariant channel model with additive Gaussian noise that may or may not be white. In [23], Leinhos assumes a Rayleigh fading model with additive white Gaussian noise (AWGN). Neither of these works takes into account the path loss in signal models, therefore their results do not reflect the dependence of the capacity on distance. The path loss effects are further taken into account in [19–21]. These works, either implicitly [19] or explicitly [21] consider an OFDM-based multi-carrier architecture and assume frequency-flat channel for each narrow sub-band. In an OFDM system, assuming that there are enough parallel channels, the frequency-selective channel effectively disintegrates into a number of frequency-flat channels and no ISI is observed. Therefore, the fading effect is modeled as a multiplicative coefficient. On the other hand, single-carrier systems over frequency-selective channels are subject to ISI which needs to be taken into account in the performance analysis.

The works which consider UWA channels with ISI are rather sparse. In [20], Choudhuri and Mitra derive capacity bounds for the UWA relay channels with ISI and investigate optimum power allocation. They however consider some idealistic

assumptions such as Thorp's path loss formula [18] which depends on only distance and frequency ignoring the effect of environmental parameters.

This thesis makes several contributions to the information theoretical performance analysis of point-to-point and relay-assisted UWA systems. A single-carrier architecture and sparse Rician frequency-selective UWA channel with ISI is considered in our work. We assume non-white Gaussian distribution to model the ambient noise [24] and consider Francois-Garrison formula [25, 26] to take into account the effects of environmental parameters such as temperature, salinity, pressure as well as distance and frequency. Exploiting the methodology introduced in [27], we develop an equivalent channel model for UWA channel with ISI and show that the capacity of the equivalent channel converges to that of the operating channel in the limit of infinite block length. Using these results, we first obtain a capacity expression for the UWA channel under consideration and demonstrate the dependency on channel parameters such as the number and location of significant taps and power delay profile and environmental parameters such as temperature, salinity, and pressure. Then, we use this expression to determine the optimal carrier frequency, input signaling, and bandwidth. A closed-form formula for the optimum carrier frequency is further obtained.

In the second part of the thesis, we extend our results to cooperative UWA systems. Considering a sparse Rician frequency-selective UWA channel with ISI, we obtain achievable rates of single-carrier cooperative UWA systems with orthogonal decode-and-forward (DF) relaying. We take into account the effect of relay geometry in the derivations of achievable rates, and use the derived expressions to optimize the location of the relay.

The rest of the thesis is organized as follows: In Chapter II, we describe the UWA channel model under consideration including path loss, fading and ambient noise for point-to-point and relay-assisted systems. In Chapter III, we investigate the information theoretical analysis and optimization of point-to-point UWA channel

with ISI. In Chapter IV, we present achievable rate, power allocation, and optimized relay location for single-carrier cooperative UWA systems with DF relaying. Finally, we conclude in Chapter V.

Notation: $(.)^T$, $(.)^*$ denote transpose and complex conjugate-transpose operations respectively. $E(.)$ denotes statistical expectation and $|.|$ denotes determinant. $*$, $\otimes$ denote linear and circular convolutions. $[x]^+$ is equivalent to $\max\{0, x\}$. $\mathbb{R}$ denotes real numbers and $\mathbb{Z}_0$ denotes the set of integers. Bold upper-case and lower-case letters denote matrices and column vectors respectively. $R_x[l] = E(x[k+l-1]\,x[k])$, $l \in \{1, 2, \ldots, N\}$ denotes the autocorrelation function of discrete signal $x[k]$, $k \in \{1, 2, \ldots, N\}$. $x[k] \overset{F}{\longleftrightarrow} x(f_n)$ denotes the Discrete Fourier Transform (DFT) of the discrete signal $x[k]$ which are the samples of the function $x(t)$. Here, $x(f_n) = \sum_{k=1}^{N} x[k]\, e^{-j2\pi(k-1)f_n}\Delta f$, $n \in \{1, 2, \ldots, N\}$, $\Delta f = 1/N$, and $f_n = (n-1)\Delta f$. $\mathbf{F}$ is defined as the DFT matrix with elements $\mathbf{F}(k, n) = (1/\sqrt{N}) \exp(-j2\pi(k-1)(n-1)/N)$ and $\forall k, n \in \{1, 2, \ldots, N\}$.

CHAPTER II

UNDERWATER ACOUSTIC CHANNEL MODEL

In this chapter, we describe the large-scale path loss, small-scale fading, and colored Gaussian noise models of UWA channels.

2.1 Path Loss

The large-scale UWA path loss is given by [19] $A(f,d) = d^s a(f)^d$ where d is the distance between the transmitter and receiver, and $1 \leq s \leq 2$ is the spreading factor which describes the geometry of propagation. Its commonly used values are $s = 2$ for spherical spreading and $s = 1$ for cylindrical spreading. $a(f)$ is the absorption coefficient which can be expressed empirically, using either Thorp's formula [18] or Francois-Garrison (FG) formula [25], [26]. According to Thorp's formula, the absorption coefficient is expressed as

$$a(f) = \frac{0.11 f^2}{1+f^2} + \frac{44 f^2}{4100+f^2} \qquad \text{dB/km} \tag{1}$$

where f is the carrier frequency (in kHz). Thorp's formula takes into account only frequency dependency of absorption coefficient while FG formula takes into accounts the environmental parameters as well. According to FG formula, the absorption coefficient is expressed as

$$a(f) = \frac{A_1 B_1 C_1 f^2}{C_1^2+f^2} + \frac{A_2 B_2 C_2 f^2}{C_2^2+f^2} + A_3 B_3 f^2 \qquad \text{dB/km} \tag{2}$$

where $A_i, i = 1,2,3$ are the temperature and salinity dependencies, $B_i, i = 1,2,3$ are the pressure dependencies, and $C_i, i = 1,2,3$ are the relaxation frequencies. In Fig. 1, Thorp's and FG formulas are compared where FG formula is plotted assuming temperature of $4°C$, salinity of 35 ppt, acidity of 8.0 pH, and depth of 1000 meter.

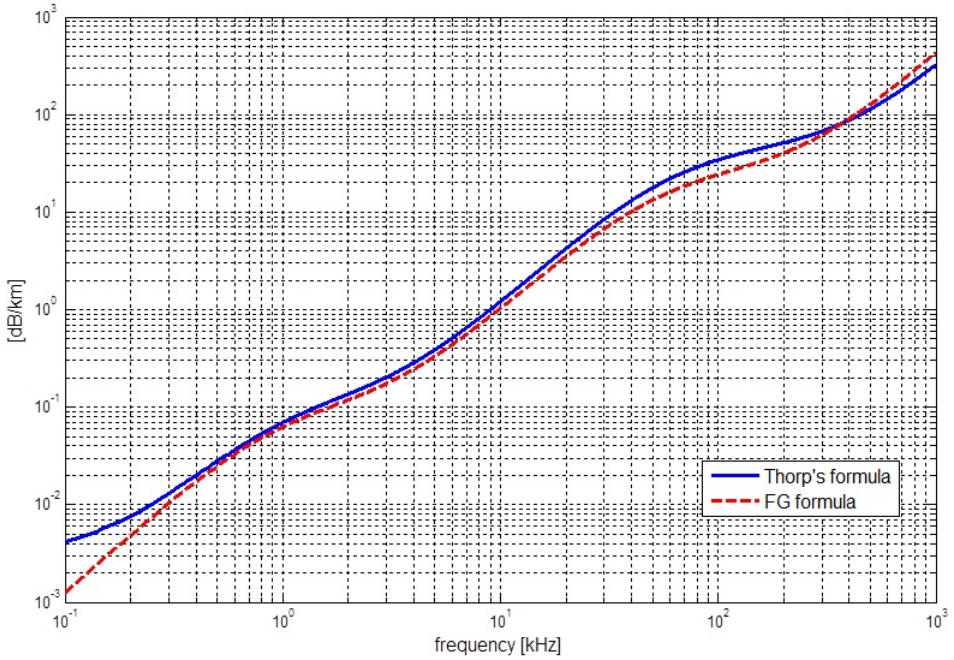

Figure 1: Comparison of Thorp and FG formulas as a function of frequency.

In a point-to-point link (which will be investigated in Chapter III), we define $G(d,f) = d^{-s}a(f)^{-d}$ as the path gain between the source and the destination (see Fig. 2.a). In a relay-assisted link (which will be explored in Chapter IV), we use d_{SD}, d_{SR}, and d_{RD} to denote the distances of source-to-destination (S $\rightarrow$ D), source-to-relay (S $\rightarrow$ R), and relay-to-destination (R $\rightarrow$ D) links respectively. Using the Pythagorean theorem, it is possible to define geometrical gains

$$G_{SD}(f) = d_{SD}^{-s}a(f)^{-d_{SD}} \tag{3}$$

$$G_{SR}(f) = \left(d_h^2 + d_r^2\right)^{-s/2}a(f)^{-\sqrt{d_h^2+d_r^2}} \tag{4}$$

$$G_{RD}(f) = \left(d_h^2 + (d_{SD}-d_r)^2\right)^{-s/2}a(f)^{-\sqrt{d_h^2+(d_{SD}-d_r)^2}} \tag{5}$$

where d_h denotes the distance of the relay node from the direct (S $\rightarrow$ D) link and d_r denotes the distance of the source node from the projection of relay node on the S $\rightarrow$ D link (see Fig. 2.b).

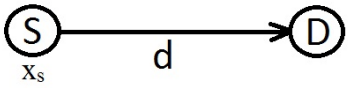

(a)

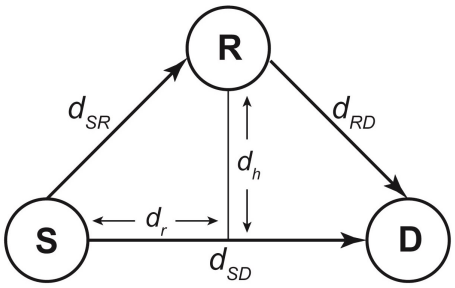

(b)

Figure 2: a) Point-to-point link, and b) Relay-assisted link.

2.2 Fading Model

The average received power is determined by the path loss, but instantaneous level of the received power fluctuates as a result of small-scale fading effects due to multipath propagation in underwater environments. The resulting frequency-selective sparse UWA channel for an X $\rightarrow$ Y link can be modeled as a finite impulse response (FIR) filter with impulse response given by[1] [28]

$$h_{XY}[k,l] = \sum_{i=1}^{L_{XY}} h_{XY,i}[k]\,\delta[l-i] \tag{6}$$

where $h_{XY,i} \overset{F}{\longleftrightarrow} h_{XY}(f_n)$, $i \in \{1,2,..,L_{XY}\}$ denote channel tap coefficients and the corresponding discrete channel frequency gains. In (6), $L_{XY} = \lceil T_d/T \rceil$ is the channel length where T_d is the delay spread, and $T \cong 1/W\ (< T_D)$ is the sampling rate of the input symbols with W denoting the transmission bandwidth.

Although there is not a general consensus within the research community on the

[1]In analysis of point-to-point links (Chapter III), the subscript XY will be dropped for simplicity.

statistical characterization of tap coefficients in UWA channels, the small-scale effects are often modeled as Rayleigh or Rician fading [29]. In this thesis, we consider Rician fading which also includes Rayleigh fading as a special case. Under Rician fading assumption, $h_{XY,i}$ is modeled as a non-zero mean complex Gaussian random process with independent real and imaginary parts having a mean of $\mu_{XY,i}/\sqrt{2}$ and a variance of $\sigma^2_{XY,i}$. The power of the i^{th} tap is therefore $\Omega_{XY,i} = E\left(|h_{XY,i}|^2\right) = \mu^2_{XY,i} + 2\sigma^2_{XY,i}$ and the normalized total power is $\sum_i \Omega_{XY,i} = 1$.

The channel power delay profile (PDP) vector is defined as $\mathbf{\Omega}_{XY} = [\Omega_{XY,1}, \Omega_{XY,2}, \ldots, \Omega_{XY,L}]$ with cardinality $|\mathbf{\Omega}_{XY}| = L_{XY}$. Since the UWA channel exhibits sparse characteristics, we further define vectors $\mathbf{\Psi}_{XY}$ and $\mathbf{\Gamma}_{XY}$ which respectively denote the PDP and the locations of significant channel taps. Their cardinality is $|\mathbf{\Psi}_{XY}| = |\mathbf{\Gamma}_{XY}| = m_{XY}$ where $m_{XY} << L_{XY}$ is the number of significant taps. Introducing the Rician factor as $k_{XY,i} = \mu^2_{XY,i}/2\sigma^2_{XY,i}$, each channel tap can be written as

$$h_{XY,i} = \sqrt{\frac{\Omega_{XY,i} k_{XY,i}}{k_{XY,i}+1}}\left(\frac{1+j}{\sqrt{2}}\right) + \sqrt{\frac{\Omega_{XY,i}}{k_{XY,i}+1}}\alpha_{XY,i} \tag{7}$$

where $\alpha_{XY,i}$ is a Gaussian random variable with zero mean and unit variance.

2.3 Ambient Noise

There are four main sources of ambient noise (turbulence, shipping, waves, and thermal noise) each of which becomes dominant in different frequency regions. The following empirical formulas give the power spectral density (PSD) of the four noise components in dB re 1 μ Pa per Hz as a function of frequency in kHz [24]:

$$10\log Z_t(f) = 17 - 30\log(f) \qquad \text{Turbulence noise} \tag{8}$$

$$10\log Z_s(f) = 40 + 20(sa - 0.5) + 26\log(f) - 60\log(f + 0.03) \qquad \text{Shipping noise} \tag{9}$$

$$10\log Z_w(f) = 50 + 7.5\omega^{1/2} + 20\log f - 40\log(f + 0.4) \qquad \text{Waves noise} \tag{10}$$

$$10\log Z_{th}(f) = -15 + 20\log(f) \qquad \text{Thermal noise} \tag{11}$$

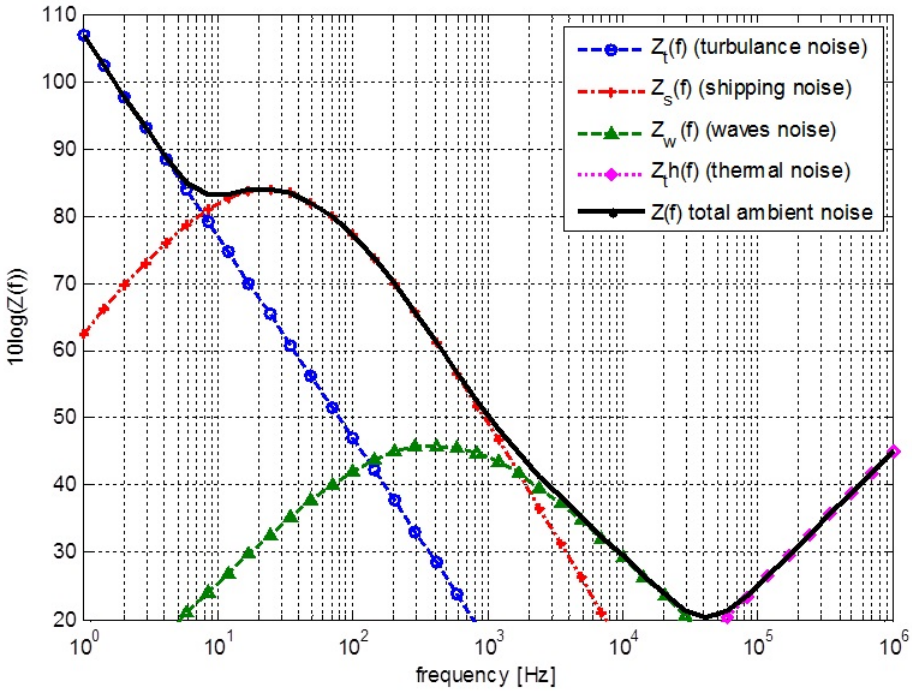

Figure 3: PSD of ambient noises and overall ambient noise ($w = 0$, $sa = 1$).

where sa is shipping activity factor and ω is the wind speed. The overall PSD of the ambient noise is given by

$$Z\left(f\right) = Z_t\left(f\right) + Z_s\left(f\right) + Z_w\left(f\right) + Z_{th}\left(f\right). \tag{12}$$

The PSD of the each noise type and the overall ambient noise are presented in Fig. 3 assuming $w = 0$ and $sa = 1$. The PSD of overall ambient noise for different values of wind speeds is further plotted in Fig. 4.

It is observed from the above figures that turbulence noise is effective in low frequency region ($f < 10$ Hz). Noise caused by shipping activities is dominant in the frequency region $10 < f < 100$ Hz and thermal noise becomes dominant in frequency region $f > 100$ kHz. Considering that most practical UWA systems operate in the frequency range of 10-100 kHz, waves' noise becomes the dominating factor. For a tractable mathematical model, PSD of waves' noise can be approximated by [17]

$$10\log Z_w\left(f\right) = 50 + 7.5\omega^{1/2} - 10\log(f^2 + f_0^2) \tag{13}$$

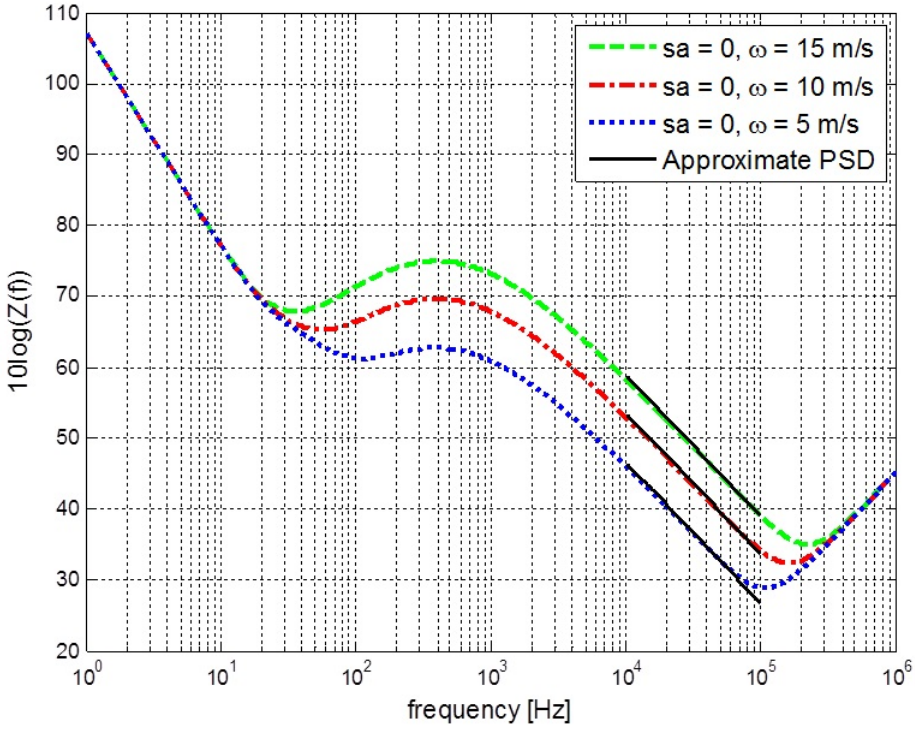

Figure 4: Overall PSD of ambient noise for different values wind speeds.

which can be rewritten as $Z_w(f) = f_0\sigma_n^2/(\pi f^2 + \pi f_0^2)$ where $\sigma^2 = E[w(t)\,w^*(t)] = (\pi 10^{5+0.75\sqrt{w}})/f_0$ and f_0 is the lowest cut-off frequency. The corresponding autocorrelation function can be then easily obtained by taking inverse Fourier transform of $Z_w(f)$ and is given by

$$R_w(\tau) = \sigma^2 \exp(-2\pi f_0 |\tau|), \forall \tau \in \mathbb{R}. \tag{14}$$

This approximate PSD is further included in Fig. 4 and provides a good match to the actual one for the frequency band of 10-100 kHz.

CHAPTER III

INFORMATION THEORETICAL PERFORMANCE ANALYSIS AND OPTIMIZATION OF POINT-TO-POINT UWA CHANNELS

In this chapter, we investigate the information theoretical limits of UWA channels. As detailed in the Chapter II, we assume a frequency-selective sparse Rician fading channel with non-white Gaussian noise and consider Francois-Garrison path loss [25, 26] to take into account the effects of environmental parameters such as temperature, salinity, pressure. Exploiting the methodology introduced in [27], we develop an equivalent channel model for UWA channel with ISI and show that the capacity of the equivalent channel converges to that of the operating channel in the limit of infinite block length. Using these results, we first obtain a capacity expression for UWA channel under consideration and then use this expression to determine the optimal carrier frequency, input signaling, and bandwidth. We further demonstrate the effect of several system and environmental parameters such as distance, temperature, depth, salinity, etc. on the capacity.

3.1 Transmission Model

Consider a transmission block size of N and let the discrete signal transmitted by the source represented by $x[k]$, $k = 1, 2, \ldots, N$. The autocorrelation function and the corresponding discrete PSD of the input signal are $R_x[k] \overset{F}{\longleftrightarrow} P(f_n)$, $k \in \{1, 2, \ldots, N\}$. The autocorrelation matrix of the input signal is therefore defined by $\mathbf{R}_x = E(\mathbf{x}\mathbf{x}^*)$

where $\mathbf{x} = (x[1], x[2], \ldots, x[N])$. The power constraint is given by

$$\frac{1}{N}\sum_{k=1}^{N} E\left(|x[k]|^2\right) \leq P_t \tag{15}$$

where NP_t is the maximum average energy allowed per block and expectation is with respect to the distributions of $x[k]$, $k = 1, 2, \ldots, N$, i.e., $p(\mathbf{x}) = \prod_{i=1}^{N} p(x[i]\,|x[i-1])$. The received signal is given by

$$y[k] = h[k,l] * g[k] * x[k] + w[k], \quad k = 1, 2, \ldots, N \tag{16}$$

where $w[k]$ is the additive non-white Gaussian noise term with autocorrelation function, and corresponding discrete PSD of $R_w[k] \overset{F}{\longleftrightarrow} Z_w(f_n)$, $k \in \{1, 2, \ldots, N\}$. Note that in the limit of $N \to \infty$, $Z_w(f_n)$ converges to $Z_w(f)$ in (13) by the definition of DFT. The autocorrelation matrix of noise signal is defined as $\mathbf{R}_w = E(\mathbf{w}\mathbf{w}^*)$ based on the discrete version of autocorrelation function given by (14). In (16), $g[k] \overset{F}{\longleftrightarrow} g(f_n)$, $k \in \{1, 2, \ldots, N\}$ represents the effect of large-scale impairments and is the discrete version of function $g(t)$ whose PSD is given by $G(f,d) = 1/A(f,d)$ (c.f. Section 2.1). In discrete time domain, it can be shown that the discretized version of the PSD, i.e. $G(f_n, d)$ is equivalent to $|g(f_n)|^2$. Under the assumption that the channel remains constant over a transmission block and replacing (6) in (16), we have

$$y[k] = \sum_{i=1}^{L} h_i (g * x)[k-i] + w[k]. \tag{17}$$

The channel in (17) is referred to as "N-block discrete-time Gaussian channel (N-DTGC)" in [27]. In the following, we exploit a technique introduced in [27] which develops an *equivalent hypothetical* circular channel model for the N-DTGC channel. This is named as "N-block Circular Gaussian Channel (N-CGC)" and shown to have the same capacity with that of N-DTGC in the limit of infinite block length. In this equivalent model, the received signal is given by

$$\begin{aligned} \bar{y}[k] &= \sum_{i=1}^{L}\sum_{j=1}^{N} h_i g[j]\, x[(k-i-j)_N] + \bar{w}[k] \\ &= h[k,l] \otimes g[k] \otimes x[k] + \bar{w}[k] \end{aligned} \tag{18}$$

where the operator $(.)_N$ is defined as

$$(k)_N = \begin{cases} k - N\left\lfloor \frac{k}{N} \right\rfloor & \text{if} \quad k \neq lN,\ l \in \mathbb{Z}_0 \\ N & \text{if} \quad k = lN,\ l \in \mathbb{Z}_0 \end{cases}. \tag{19}$$

In (18), $\bar{w}[k]$ is additive non-white Gaussian noise term with periodic autocorrelation function [30] given by $R_{\bar{w}}[k] = E(\bar{w}[k]\,\bar{w}[j]) = R_w[k-j]+R_w[k-j+N]+R_w[k-j-N]$ and $R_{\bar{w}}[k] \overset{F}{\longleftrightarrow} Z_{\bar{w}}(f_n)$, $k, j \in \{1, 2, \ldots, N\}$. Noting that it is a periodic repetition of R_w and noise samples from different blocks are independent, we have $R_{\bar{w}}[k] = R_w[k]$ and $Z_{\bar{w}}(f_n) = Z_w(f_n)$ for $\forall n \in \{1, 2, \ldots, N\}$.

The output sequence in vector form is given by

$$\bar{\mathbf{y}} = \mathbf{CHx} + \bar{\mathbf{w}} \tag{20}$$

where $\bar{\mathbf{y}} = (\bar{y}[1], \bar{y}[2], \ldots, \bar{y}[N])$ and $\bar{\mathbf{w}} = (\bar{w}[1], \bar{w}[2], \ldots, \bar{w}[N])$. In (20), $\mathbf{C}$ and $\mathbf{H}$ are circulant matrices with elements $[\mathbf{H}]_{i,j} = h_{(j-i+1)_N}$ and $[\mathbf{C}]_{i,j} = g[(j-i+1)_N]$. Note that circulant matrices can be diagonalized by DFT matrix $\mathbf{F}$. Let us define $\bar{\mathbf{Y}} = \mathbf{F}\bar{\mathbf{y}}$, then we have

$$\bar{\mathbf{Y}} = \mathbf{GDX} + \bar{\mathbf{W}} \tag{21}$$

where $\mathbf{G} = \mathbf{FCF}^*$, $\mathbf{D} = \mathbf{FHF}^*$, $\mathbf{X} = \mathbf{Fx}$, and $\bar{\mathbf{W}} = \mathbf{F}\bar{\mathbf{w}}$. Note that $\mathbf{G}$ and $\mathbf{D}$ are diagonal matrices with diagonal elements $\mathbf{G}_{nn} = \sum_{k=1}^{N} g[k]\, e^{-j2\pi(k-1)(n-1)/N}\Delta f$ and $\mathbf{D}_{nn} = \sum_{i=1}^{L} h_i e^{-j2\pi(i-1)(n-1)/N}\Delta f$ or, equivalently, $\mathbf{G}_{nn} = g(f_n)$ and $\mathbf{D}_{nn} = h(f_n)$.

3.2 Capacity Analysis

In this section, we first present the derivation of instantenous channel capacity for a given realization of the fading channel. Then, performing an expectation over the fading distrubution, we obtain average channel capacity.

The equivalent N-CGC model decomposes the multipath channel into a set of N parallel Gaussian channels via DFT decomposition. Considering the input-output

relation in (21) and noting that the linear DFT operation does not affect the information rate of the channel, the capacity of N-CGC is given by

$$C_N^c = \sup_{p(\mathbf{x})} \frac{1}{N} I\left(\mathbf{X}; \bar{\mathbf{Y}}\right). \tag{22}$$

The capacity of the N-DTGC under consideration can then be found by letting $N \to \infty$, i.e.,

$$C = \lim_{N\to\infty} C_N^c = \lim_{N\to\infty} \sup_{p(\mathbf{x})} \frac{1}{N} I\left(\mathbf{X}; \bar{\mathbf{Y}}\right) \tag{23}$$

where the maximization is taken over the input distribution. The mutual information is given by

$$I\left(\mathbf{X}; \bar{\mathbf{Y}}\right) = \mathcal{H}\left(\bar{\mathbf{Y}}\right) - \mathcal{H}\left(\bar{\mathbf{Y}}|\mathbf{X}\right) \tag{24}$$

where $\mathcal{H}(.)$ is differential entropy. Replacing (21) in (24), we have

$$\begin{aligned} I\left(\mathbf{X}; \bar{\mathbf{Y}}\right) &= \mathcal{H}\left(\mathbf{GDX} + \bar{\mathbf{W}}\right) - \mathcal{H}\left(\bar{\mathbf{W}}\right) \\ &\leq \frac{1}{2} log 2\pi e \left|\mathbf{GDK_X D^* G^*} + \mathbf{K}_{\bar{\mathbf{W}}}\right| - \frac{1}{2} log 2\pi e \left|\mathbf{K}_{\bar{\mathbf{W}}}\right| \end{aligned} \tag{25}$$

where $\mathbf{K_X} = E\left(\mathbf{XX}^*\right) = \mathbf{F R}_x \mathbf{F}^*$ and $\mathbf{K}_{\bar{\mathbf{W}}} = E\left(\bar{\mathbf{W}}\bar{\mathbf{W}}^*\right) = \mathbf{F R}_{\bar{w}} \mathbf{F}^*$ are, respectively, the DFT of input and noise autocorrelation matrices. Due to the periodic property of autocorrelation function $R_{\bar{w}}[k]$, the autocorrelation matrix $\mathbf{R}_{\bar{w}}$ is circulant. Hence, $\mathbf{R}_{\bar{w}}$ can be diagonalized by the DFT which results in the diagonality of $\mathbf{K}_{\bar{\mathbf{W}}}$. The inequality comes from the fact that Gaussian distribution of input maximizes the entropy.

Hadamard's inequality [31] implies that diagonal $\mathbf{K_X}$ maximizes the mutual information. Therefore, (25) is further upper bounded by

$$I\left(\mathbf{X}; \bar{\mathbf{Y}}\right) \leq \frac{1}{2} \sum_{n=1}^{N} \log\left(1 + \frac{|\mathbf{G}_{nn}|^2 |\mathbf{D}_{nn}|^2 \mathbf{K_X}_{nn}}{\mathbf{K}_{\bar{\mathbf{W}}nn}}\right) \tag{26}$$

where $\mathbf{K_X}_{nn} = \sum_{k=1}^{N} R_x[k]\, e^{-j2\pi(k-1)(n-1)/N} \Delta f$ and $\mathbf{K}_{\bar{\mathbf{W}}nn} = \sum_{k=1}^{N} R_{\bar{w}}[k]\, e^{-j2\pi(k-1)(n-1)/N} \Delta f$ are the diagonal components of $\mathbf{K_X}$ and $\mathbf{K}_{\bar{\mathbf{W}}}$ and correspond to the discrete values of input signal PSD and noise PSD, i.e., $\mathbf{K_X}_{nn} = P(f_n)$, $\mathbf{K}_{\bar{\mathbf{W}}nn} = Z_w(f_n)$. In (26), we

replace $|\mathbf{G}_{nn}|^2$ and $|\mathbf{D}_{nn}|^2$ with $G(f_n, d)$ and $|h(f_n)|^2$ respectively. We can therefore rewrite the capacity as

$$C = \lim_{N\to\infty} \max_{P(f_n)} \frac{1}{2N} \sum_{n=1}^{N} \log\left(1 + \frac{G(f_n, d)\,|h(f_n)|^2 P(f_n)}{Z_w(f_n)}\right)$$
$$\text{subject to } \frac{1}{N}\sum_{n=1}^{N} P(f_n) \le P_t. \tag{27}$$

As the number of sub-bands N grows, the frequency width, i.e., Δf, goes to zero in the limit of $N \to \infty$, and they represent a finer sampling of the continuous spectrum. Then (27) converges to

$$C = \max_{P(f)} \frac{1}{2} \int_{-1/2}^{1/2} \log\left(1 + \frac{G(f, d)\,|h(f)|^2 P(f)}{Z_w(f)}\right) df \qquad \text{bits/sec/Hz}$$
$$\text{subject to } \int_{-1/2}^{1/2} P(f) df \le P_t. \tag{28}$$

Considering a carrier frequency f_c and a specific bandwidth W, the capacity of the link in bits/sec can be found with the same procedure by replacing $\Delta f = W/N$ in the definition of DFT. Capacity in bits/sec is therefore obtained as

$$C = \max_{P(f)} \frac{1}{2} \int_{W} \log(1 + SNR(f))\, df$$
$$\text{subject to } \frac{1}{W}\int_{W} P(f) df \le P_t. \tag{29}$$

Here, the integration is over the operating band and the narrowband SNR is defined as $SNR(f) = G(f, d)\,|h(f)|^2 P(f)/Z_w(f)$. It is worth mentioning that the above capacity expression also includes Gaussian channel with *no ISI*, i.e., $|h(f)|^2 = 1$, and *frequency-flat* Rician fading channel, i.e., $|h(f)|^2 = |h_1|^2$, as special cases.

The expression in (29) is provided for a given realization of the channel. To find the average capacity, one needs to take expectation of (29) with respect to the distribution of $|h(f)|^2$. $h(f)$ is the Fourier Transform of the discrete channel taps, i.e., $h(f) = \sum_{i=1}^{L} h_i e^{-j2\pi f(i-1)}$ where h_i's are complex Gaussian random processes with independent real and imaginary parts having a mean of $\mu_i/\sqrt{2}$ and a variance

of σ_i^2 (c.f. Section 2.2). Since $h(f)$ is a linear summation of independent complex Gaussian random processes, it is also a complex Gaussian random process with mean $\mu(f) = \sum_{i=1}^{L} E(h_i) e^{-j2\pi f(i-1)}$ and variance $\sigma_h^2 = \sum_{i=1}^{L} 2\sigma_i^2$. Considering that $\sum_i (\mu_i^2 + 2\sigma_i^2) = 1$ (c.f. Section 2.2), it is easy to show that $|h(f)|^2$ follows the exponential pdf [32]

$$p\left(|h(f)|^2\right) = \frac{1}{1+\lambda} \exp\left(-\frac{|h(f)|^2}{1+\lambda}\right)$$

where λ is defined as

$$\lambda = 2\sum_{i=1}^{L} \sum_{j=i+1}^{L} \mu_i \mu_j \cos\left(2\pi f (j-i)\right). \tag{30}$$

Under the assumption that channel state information (CSI) is only available at the receiver side, the source allocates equal power across the subbands since there is no knowledge of the channel at the transmitter side. Setting $P(f) = P_t$ in (29), we need to calculate

$$\bar{C} = E_{|h(f)|^2}\left(\frac{1}{2}\int_W \log\left(1 + \frac{G(f,d)\,P_t}{Z_w(f)}|h(f)|^2\right) df\right). \tag{31}$$

Assuming $\rho = |h(f)|^2/(1+\lambda)$, (31) can be written as

$$\bar{C} = \frac{1}{2}\int_W \int_0^{\infty} \log\left(1 + \frac{(1+\lambda)\,G(f,d)\,P_t}{Z_w(f)}\rho\right) \exp(-\rho) d\rho df. \tag{32}$$

Using the results of [32], we can rewrite (32) as

$$\bar{C} = \frac{\log_2(e)}{2}\int_W \exp\left(\frac{Z_w(f)}{(1+\lambda)\,G(f,d)\,P_t}\right) \Gamma\left(0, \frac{Z_w(f)}{(1+\lambda)\,G(f,d)\,P_t}\right) df \tag{33}$$

where $\Gamma(a,z) = \int_z^{\infty} t^{a-1} e^{-t} dt$ denotes the *incomplementary gamma function* [32]. Using the first series expansion of $\Gamma(0,z)$ [32,33] and substituting it in (33), we have

$$\bar{C} = \frac{\log_2(e)}{2}\int_W \exp\left(\frac{Z_w(f)}{(1+\lambda)\,G(f,d)\,P_t}\right)\left[-\gamma + \ln\left(\frac{(1+\lambda)\,G(f,d)\,P_t}{Z_w(f)}\right) - \sum_{k=1}^{\infty} \frac{1}{k.k!}\left(\frac{-Z_w(f)}{(1+\lambda)\,G(f,d)\,P_t}\right)^k\right] df \tag{34}$$

where γ is the Euler constant ($\gamma = 0.577215665$). At high SNR values, (34) can be approximated as

$$\bar{C} \simeq \frac{\log_2(e)}{2} \int_W \exp\left(\frac{Z_w(f)}{(1+\lambda)\,G(f,d)\,P_t}\right)\left[-\gamma + \ln\left(\frac{(1+\lambda)\,G(f,d)\,P_t}{Z_w(f)}\right) + \frac{Z_w(f)}{(1+\lambda)\,G(f,d)\,P_t}\right] df \tag{35}$$

3.3 Effect of Channel Parameters on the Average Capacity

In this section, we investigate the effect of PDP and location of significant channel taps on the average capacity.

3.3.1 Effect of significant taps' locations

Note that the term λ defined in (30) contains all the information about PDP and location of significant taps. It can be readily verified that we will have $\lambda = 0$ for a frequency-flat channel. Considering the expression of average capacity in (34), we observe that the term $1+\lambda$ is multiplied to the transmit power, meaning that PDP and taps' location will affect the received power through this term. Therefore, in order to understand the effect of PDP and taps' location on the capacity, we investigate the behaviour of the term $1+\lambda$.

Recall from Chapter II that $\mathbf{\Gamma} = [\Gamma_1, \Gamma_2, ..., \Gamma_m]$ defines the location vector of significant taps. Therefore, we can rewrite (30) as

$$1 + \lambda = 1 + 2\sum_{i=1}^{m}\sum_{j=i+1}^{m} \mu_{\Gamma_i}\mu_{\Gamma_j}\cos\left(2\pi f\left(\Gamma_j - \Gamma_i\right)\right). \tag{36}$$

After some mathematical manipulations, we obtain

$$1 + \lambda = \frac{1}{1+k} + \left(\sum_{i=1}^{m}\mu_{\Gamma_i}\cos\left(2\pi\Gamma_i f\right)\right)^2 + \left(\sum_{i=1}^{m}\mu_{\Gamma_i}\sin\left(2\pi\Gamma_i f\right)\right)^2 \tag{37}$$

where k is the Rician factor. Using Cauchy-Schwarz inequality, we can find bounds on $1+\lambda$ as

$$\frac{1}{1+k} \leq 1 + \lambda \leq \frac{1+mk}{1+k}. \tag{38}$$

Assume uniform PDP (i.e. $\Omega_i = 1/m$). Consequently we can write

$$\mu_{\Gamma_i} = \sqrt{\frac{k}{m\,(1+k)}} \quad \text{for} \quad \forall i. \tag{39}$$

Under the assumption that difference between the locations of two consequence channel taps is constant and equal to r (i.e. $\Gamma_{i+1} - \Gamma_i = r$ for $\forall i$), we can rewrite (37) as

$$1 + \lambda = \frac{1}{k+1} + \left(\frac{k}{m\,(k+1)}\right) \frac{1 - \cos\left(m 2\pi r f\right)}{1 - \cos\left(2\pi r f\right)}. \tag{40}$$

The minimum and maximum values of (40) are found as

$$\min\left\{1 + \lambda\right\} = \frac{1}{k+1} \tag{41}$$

$$\max\left\{1 + \lambda\right\} = \frac{1}{k+1} + \left(\frac{k}{m\,(k+1)}\right) \underbrace{\max\left\{\frac{1 - \cos\left(m 2\pi r f\right)}{1 - \cos\left(2\pi r f\right)}\right\}}_{m^2} \tag{42}$$

The maximum value takes place when $1 - \cos\left(2\pi r f\right) = 0$. For $0 \leq f \leq 1$, the solution is $f = i/r$, $i = 0, 1, 2, ..., r$ and the number of peaks is equal to $r + 1$. As r increases, the number of peaks in $1 + \lambda$ increases, therefore, the capacity increases. As a conclusion, we can state that, under the assumption of uniform PDP, as the spacing between significant taps increases, capacity increases and becomes closer to the capacity of frequency-flat channel.

3.3.2 Effect of PDP

The PDP vector of significant taps $\mathbf{\Psi} = [\Psi_1, \Psi_2, ..., \Psi_m]$ is related to $1 + \lambda$ by

$$\mu_{\Gamma_i} = \sqrt{\frac{k\Psi_i}{k+1}}. \tag{43}$$

Replacing this in (37), we have

$$1+\lambda = \frac{1}{1+k} + \frac{k}{1+k}\left(\sum_{i=1}^{m} \sqrt{\Psi_i} \cos\left(2\pi\Gamma_i f\right)\right)^2 + \frac{k}{1+k}\left(\sum_{i=1}^{m} \sqrt{\Psi_i} \sin\left(2\pi\Gamma_i f\right)\right)^2. \tag{44}$$

It can be argued that, in most cases, the power of earlier taps are stronger than the later ones since later taps experience more delay and more attenuation (i.e. $\Psi_1 \geq$

$\Psi_2 \geq \cdots \geq \Psi_m$). Therefore, we can use Chebyshev's Inequality and write

$$\left(\sum_{i=1}^{m} \sqrt{\Psi_i} \cos\left(2\pi\Gamma_i f\right)\right)^2 \geq \left(\sum_{i=1}^{m} \sqrt{\Psi_i}\right)^2 \left(\sum_{i=1}^{m} \cos\left(2\pi\Gamma_i f\right)\right)^2 \tag{45}$$

$$\left(\sum_{i=1}^{m} \sqrt{\Psi_i} \sin\left(2\pi\Gamma_i f\right)\right)^2 \geq \left(\sum_{i=1}^{m} \sqrt{\Psi_i}\right)^2 \left(\sum_{i=1}^{m} \sin\left(2\pi\Gamma_i f\right)\right)^2. \tag{46}$$

This lets us write a lower bound on (44) as

$$1 + \lambda \geq \frac{1}{1+k} + \frac{k}{1+k}\left(\sum_{i=1}^{m} \sqrt{\Psi_i}\right)^2 \left[\left(\sum_{i=1}^{m} \cos\left(2\pi\Gamma_i f\right)\right)^2 + \left(\sum_{i=1}^{m} \sin\left(2\pi\Gamma_i f\right)\right)^2\right]. \tag{47}$$

Furthermore, since $0 \leq \Psi_i \leq 1$ for $\forall i$, we have

$$\left(\sum_{i=1}^{m} \sqrt{\Psi_i}\right)^2 \geq \sum_{i=1}^{m} \left(\sqrt{\Psi_i}\right)^2 = 1 \tag{48}$$

and (47) is further lower bounded as

$$1 + \lambda \geq \frac{1}{1+k} + \frac{k}{1+k}\left[\left(\sum_{i=1}^{m} \cos\left(2\pi\Gamma_i f\right)\right)^2 + \left(\sum_{i=1}^{m} \sin\left(2\pi\Gamma_i f\right)\right)^2\right] \tag{49}$$

where the equlity holds if $\Psi_1 = \Psi_2 = \cdots = \Psi_m = 1/m$ (i.e., uniform PDP).

Assuming that taps are located at equal distances of r, the right hand side of above inequality can be written as

$$1 + \lambda \geq \frac{1}{k+1} + \left(\frac{k}{m\left(k+1\right)}\right) \frac{1 - \cos\left(m2\pi r f\right)}{1 - \cos\left(2\pi r f\right)} \tag{50}$$

which yields the formula in (40) obtained under the assumption of uniform PDP in the previous subsection.

Our results indicate that uniform PDP results in the lowest capacity among different PDP types. Furthermore, it is observed from (44) that when more power is localized at a small number of taps, capacity increases and becomes closer to the capacity of frequency-flat channel in which all of the power is localized at only one tap.

3.4 Numerical Results

In this section, we present numerical results for the derived expressions within this chapter. Unless otherwise noted, we have the following assumptions: We consider a carrier frequency of 30 kHz and a transmission distance of $d = 1$ km. We assume temperature $T = 22°$C, depth $D = 50$ m, acidity of 8 pH, salinity $S = 35$ ppt, wind speed $\omega = 0$ m/s and spreading factor $s = 1.5$. We assume that the UWA channel experiences a multipath delay spread of 13 ms and has the order of $L = 130$. The number of significant delay taps is $m = 10$ and located at equal distances from each other with a uniform PDP, i.e., the power of each significant tap is $1/m$[1] . The Rician k factor for the significant taps is 2 dB.

Accuracy of derived expression: In an effort to demonstrate the accuracy of derived expression for average channel capacity, we plot (34) and compare it with the numerical evalution of (29). In the calculation of (34), first hundred terms of the series are considered. It is observed from Fig. 5 that the derived expression coincides perfectly with the numerical results.

Effect of ISI and distance: In Fig. 6, we present the capacity as a function of SNR for different link distances. As benchmarks, the capacity of AWGN and frequency-flat Rician fading channel are also depicted in this figure. Comparison with frequency-flat case under the assumptions of same colored noise and path loss reveals that the presence of ISI reduces the capacity. Specifically, at SNR=20 dB, a capacity of 3.19 bits/s/Hz is achieved for $d = 1$ km over frequency-flat Rician fading channel. This reduces to 2.78 bits/s/Hz over frequency-selective channel for the same link distance. It is further observed that an increase in distance would result in a decrease in capacity as expected. Specifically, at SNR=20 dB, a capacity of 2.78 bits/s/Hz is achieved for $d = 1$ km. This reduces to 2.45 bits/s/Hz for $d = 2$ km. It

[1]Since the total power of channel taps is normalized to 1, i.e. $\sum_i \Omega_i = 1$.

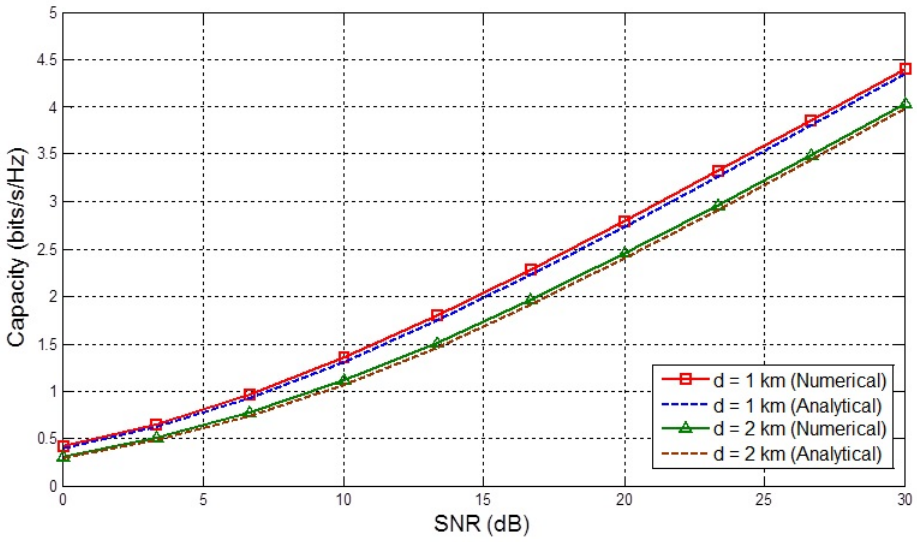

Figure 5: Comparison of derived expressions for average channel capacity vs. numerical results.

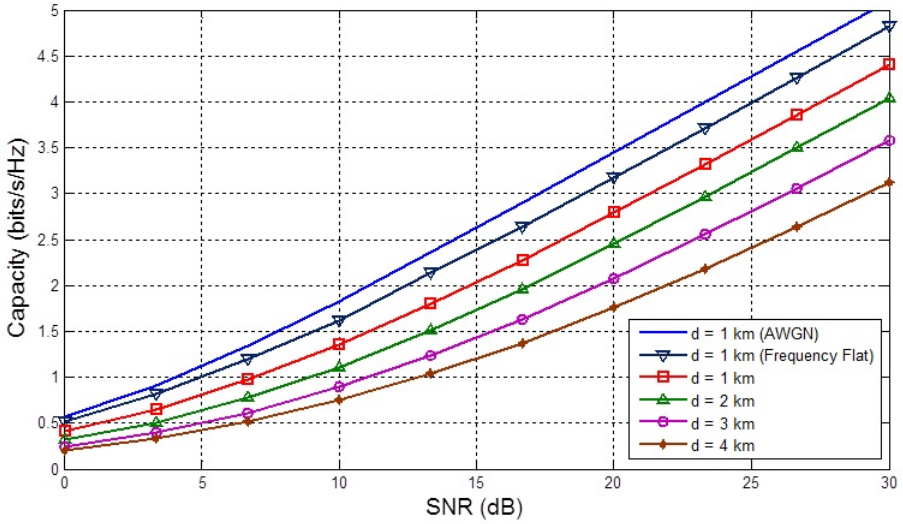

Figure 6: Capacity as a function of SNR for different link distances.

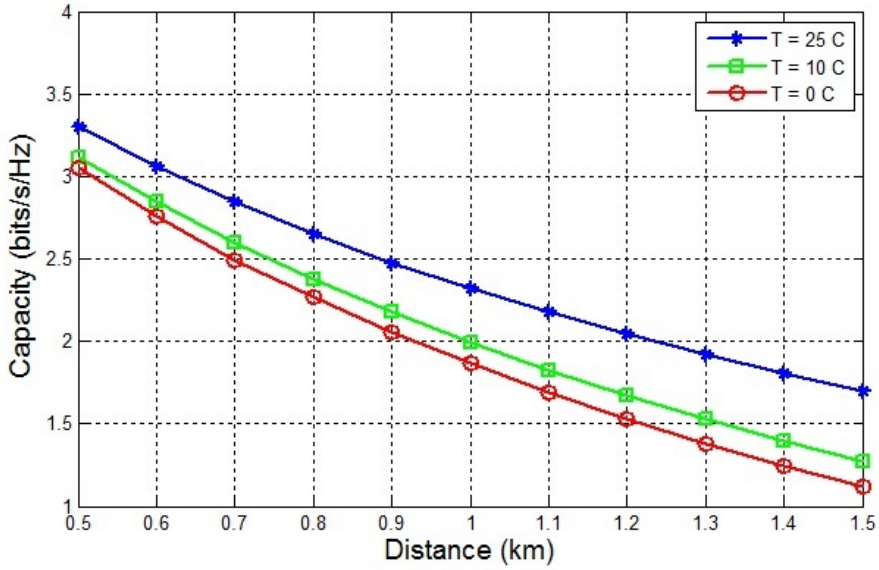

Figure 7: Capacity vs. distance for different temperature values (SNR=20 dB).

further reduces to 2.07 and 1.75 bits/s/Hz, respectively for $d = 3$ km and $d = 4$ km.

Effect of temperature and depth: In Fig. 7 and 8, we study the effect of temperature and depth on the capacity. In Fig. 7, we consider three temperatures, namely 0°C, 10°C and 25°C. We observe that for a distance of $d = 1$ km, the lowest capacity among three cases is achieved for 0°C. Specifically, a capacity of 1.86 bits/s/Hz is obtained. This climbs up to 2.00 bits/s/Hz for 10°C and 2.32 bits/s/Hz for 25°C. Our results demonstrate that higher underwater temperature is more favorable for acoustic transmission. In Fig. 8, we assume a fixed temperature of 25°C and consider depths of 50 m, 500 m, and 1 km. We observe that an increase in depth will result in an increase in capacity as well. However, this increase is not noticeable in comparison to the wider variation of capacity with respect to temperature.

Effect of salinity: In Fig. 9, we investigate the effect of salinity on the capacity. Specially, we consider salinity of 30 ppt and 35 ppt. We observe that the capacity for salinity of 30 ppt (assuming $d = 1$ km) is 2.39 bits/s/Hz which is more than the capacity obtained for salinity of 35 ppt.

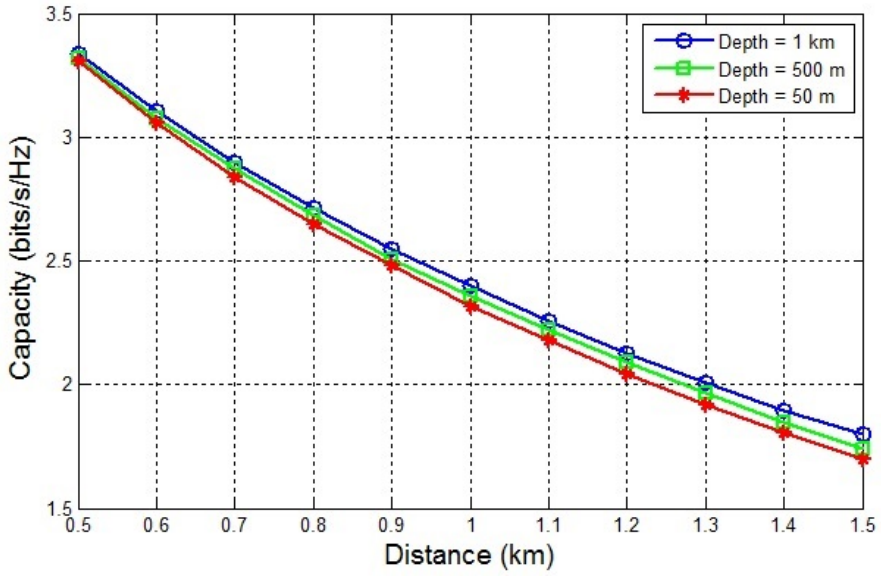

Figure 8: Capacity vs. distance for different values of depth (SNR=20 dB).

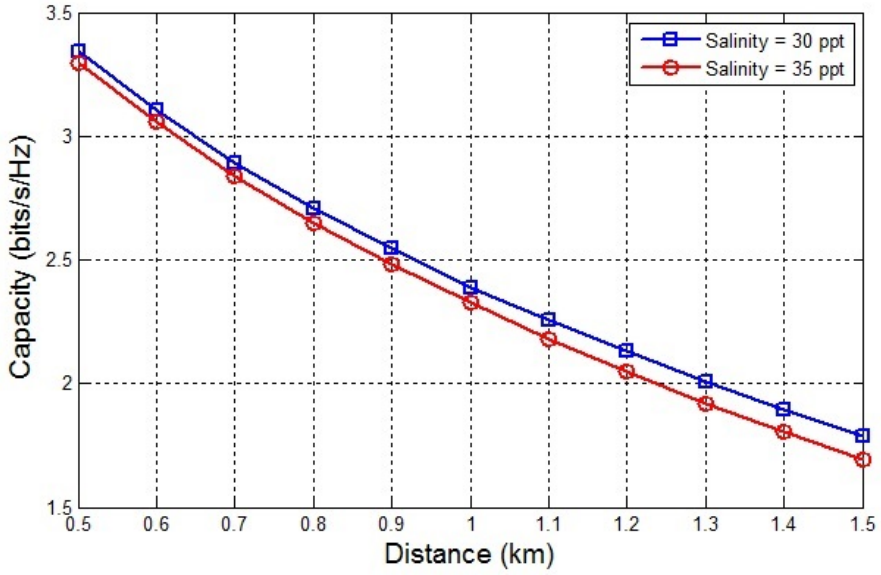

Figure 9: Capacity vs. distance for different values of salinity (SNR=20 dB).

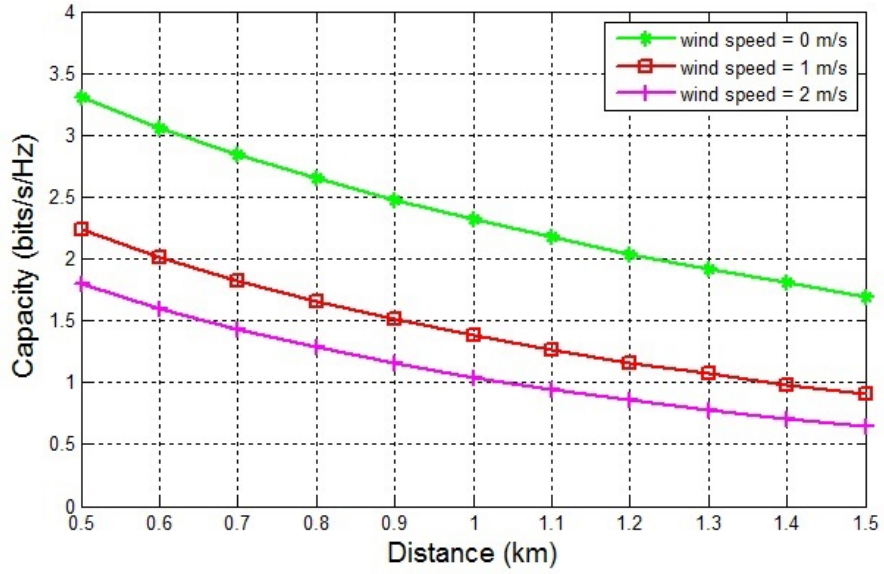

Figure 10: Capacity vs. distance for different wind speeds (SNR=20 dB).

Effect of wind speed: In Fig. 10, we examine the capacity for wind speeds of 0, 1, and 2 m/s . The highest capacity among these three cases is achieved when the wind speed is zero. Specifically, a capacity of 2.32 bits/s/Hz is achieved for $\omega = 0$ m/s. This reduces to 1.38 bits/s/Hz for $\omega = 1$ m/s and further reduces to 1.04 bits/s/Hz for $\omega = 2$.

Effect of taps' locations: In Fig. 11, we investigate the effect of significant channel taps' locations on the capacity. We assume ten significant taps (i.e., $m = 10$) with uniform PDP and consider the following $\mathbf{\Gamma}$ vectors to indicate the location of significant taps:

- $\mathbf{\Gamma}_1 = [1, 2, 3, 4, 5, 6, 7, 8, 9, 10]$, (i.e., the locations of significant taps are consecutive)
- $\mathbf{\Gamma}_2 = [1, 2, 3, 4, 5, 6, 7, 8, 11, 20]$
- $\mathbf{\Gamma}_3 = [1, 2, 3, 4, 5, 6, 11, 20, 47, 128]$
- $\mathbf{\Gamma}_4 = [1, 15, 29, 43, 57, 71, 85, 99, 113, 127]$, (i.e., equally spaced taps)

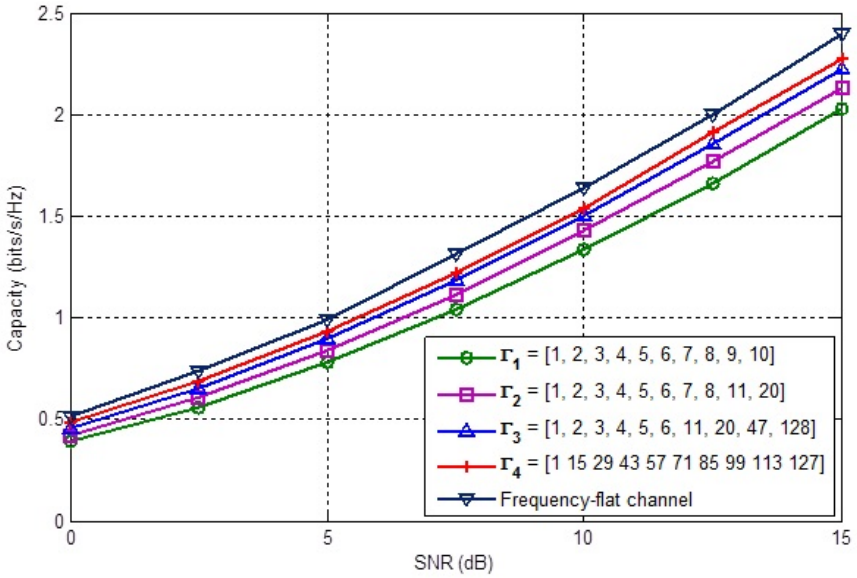

Figure 11: Capacity vs. SNR for different locations of significant taps ($d = 1$ km).

It is observed from Fig. 11 that as the spacing between significant taps increases, capacity becomes closer to the capacity of frequency-flat channel. For example, in a channel with $\mathbf{\Gamma}_1$, a capacity of 1.27 bits/s/Hz is achieved at dB. This climbs up to 1.49 bits/s/Hz for a channel with $\mathbf{\Gamma}_3$, where the spacing between the significant taps is more. This further increases to 1.54 bits/s/Hz for $\mathbf{\Gamma}_4$ which is the case of equal spacing. These observations further confirm the concluding remarks of Section 3.3 which states that capacity increases as the spacing between significant taps (r) increases. Specifically, in a channel with $\mathbf{\Gamma}_1$ with $r = 1$, the lowest capacity is achieved. On the other hand, for the case of $\mathbf{\Gamma}_4$ with $r = 14$, the capacity increases and becomes closer to the capacity of frequency-flat channel.

Effect of PDP: In Fig. 12, we study the effect of significant channel taps' PDP on the capacity. Assuming $m = 10$, we consider the following PDPs:

- $\mathbf{\Psi}_1 = [1]$, (i.e., frequency-flat Rician fading channel)
- $\mathbf{\Psi}_2 = [.7,\ .1,\ .025,\ .025,\ .025,\ .025,\ .025,\ .025,\ .025,\ .025]$

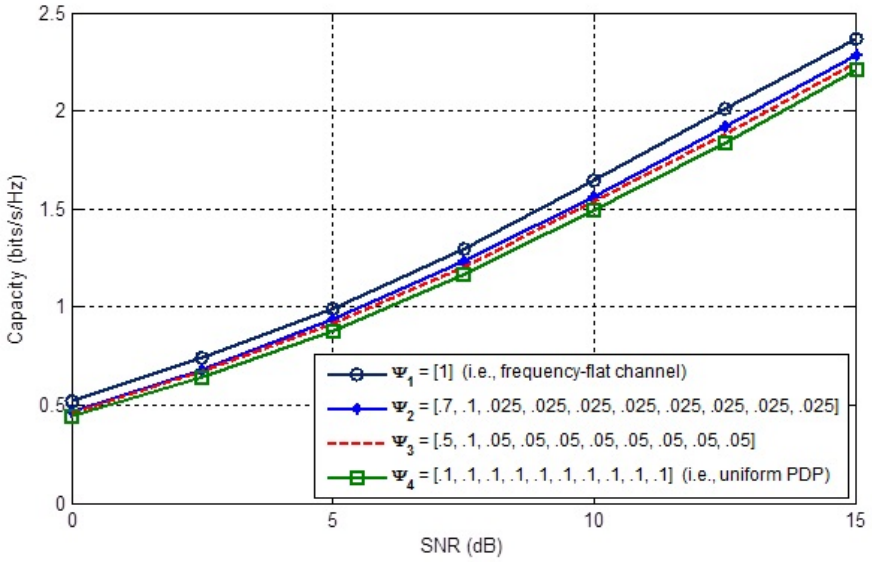

Figure 12: Effect of PDP of significant taps on the capacity ($d = 1$ km).

- $\mathbf{\Psi}_3 = [.5,\ .1,\ .05,\ .05,\ .05,\ .05,\ .05,\ .05,\ .05,\ .05]$
- $\mathbf{\Psi}_4 = [.1,\ .1,\ .1,\ .1,\ .1,\ .1,\ .1,\ .1,\ .1,\ .1]$, (i.e., uniform PDP)

Our results demonstrate that uniform PDP results in the lowest capacity among the considered PDPs. This confirms our observations in Section 3.3 which states that under the assumption of equally spaced taps, uniform PDP results in lowest capacity as $\mathbf{\Psi}_4$ does in Fig. 12. It is also observed that when more power is localized at a small number of taps (c.f., $\mathbf{\Psi}_3$, $\mathbf{\Psi}_2$) capacity increases and becomes closer to the capacity of frequency-flat channel (i.e. $\mathbf{\Psi}_1$) as discussed in Section 3.3.

Effect of the number of significant channel taps: In Fig. 13, we examine the effect of the number of significant channel taps on the capacity. We consider, $m =$ 2, 4, 6, 8, 10 and 20 and assume that significant taps are located at equal distances from each other with a uniform PDP. As limiting cases, we also include the case of $m = 1$ (i.e., frequency-flat channel) and $m = L = 130$ (i.e., non-sparse channel). It is observed that as the number of significant taps increases and the total power is spread over many taps, the capacity decreases. This is expected as discussed in Section 3.3.

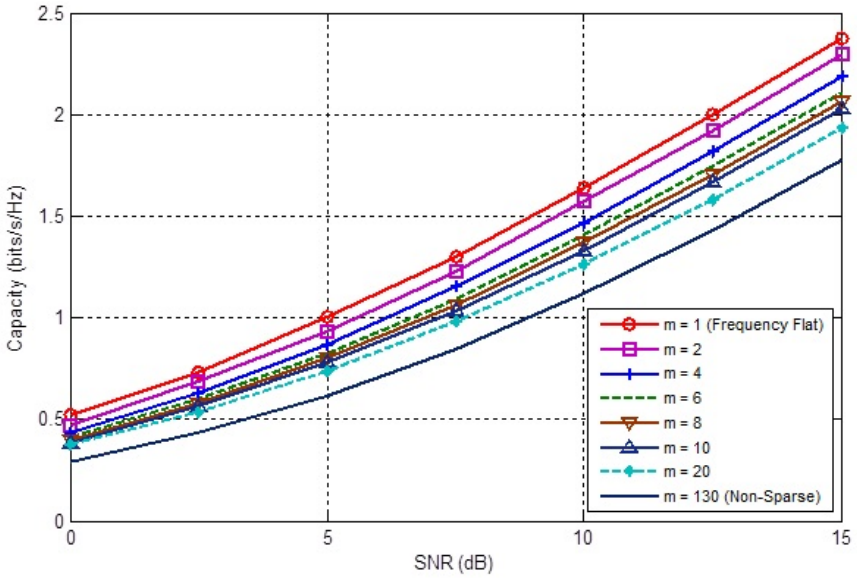

Figure 13: Capacity vs. SNR for different numbers of significant taps ($d = 1$ km).

It can be checked from (40) that when m increases, the term $1 + \lambda$ decreases and, consequently, the capacity also decreases.

3.5 Capacity Optimization

In this section, we aim to determine carrier frequency, input signal PSD, and bandwidth as to optimize the capacity.

3.5.1 Choice of Optimal Frequency

Maximization of the channel capacity in (29) with respect to carrier frequency is equivalent to maximizing $G(f,d)/Z_w(f)$. Recalling the definition of the path gain and differentiating the resulting expression with respect to f and setting it to zero, we have

$$d\frac{\partial a(f)_{\mathrm{dB}}}{\partial f} + \frac{\partial Z_w(f)_{\mathrm{dB}}}{\partial f} = 0. \tag{51}$$

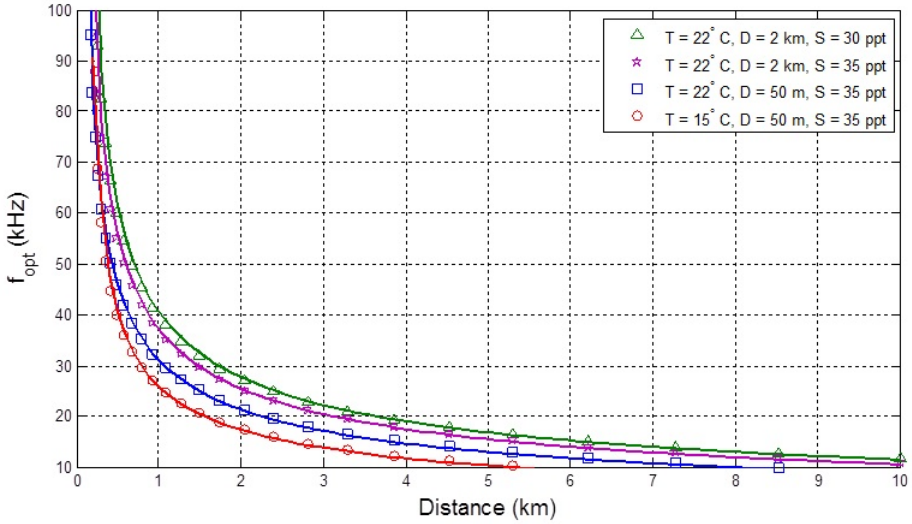

Figure 14: Optimal carrier frequency f_{opt} in terms of environmental parameters. Solid lines indicate the approximation formula given by (52).

After some mathematical manipulations (see Appendix A), we find the optimal frequency as

$$f_{\text{opt}} \cong \sqrt{\frac{367.5}{\frac{S}{35}\left(1+\frac{T}{43}\right)\exp\left(-\frac{D}{6}-\frac{T}{17}\right)d - 0.28\exp\left(-\frac{2T}{17}\right)}} \tag{52}$$

where S, D, and T represent the salinity, depth, and temperature respectively.

The optimal frequency as a function of transmission distance is illustrated in Fig. 14 for different values of temperature, depth and salinity. It is also observed that direct numerical solution of (51) and the derived approximate closed-form solution in (52) provide a perfect match. Assuming temperature of 22°C, depth of 50 m, and salinity of 35 ppt, the optimal frequencies are found to be 55, 30, 21.37, and 17.17 kHz respectively for distances of d =350 m, 1 km, 2 km, and 3 km. This indicates that the optimal frequency decreases with increasing range.

Furthermore, we consider four cases to demonstrate the effect of temperature, depth and salinity on the optimal frequency. It is observed from Fig. 14 that an increase in temperature and/or depth results in an increase in optimal frequency, while an increase in salinity results in a decrease in optimal frequency. For example, at 22°C, depth of 50 m, and salinity of 35 ppt, the optimal frequency is 30 kHz for

$d = 1$ km. Keeping temperature and salinity fixed and changing the depth from 50 m to 2 km, the optimal frequency increases from 30 to 37 kHz. Keeping temperature and depth fixed and changing the salinity from 30 to 35 ppt, the optimal frequency reduces from 40 to 37 kHz. On the other hand, keeping depth and salinity fixed and changing the temperature from 15°C to 22°C , the optimal frequency increases from 25 to 30 kHz.

3.5.2 Optimal Power Allocation

If the CSI is present at both transmitter and receiver side, we can maximize the capacity with respect to the PSD of input signal. A direct maximization of (28) appears to be intractable. By equivalency of (27) and (28), we reconsider the power allocation problem in the continuous frequency domain via a finite dimension domain. We then take the limit as $N \to \infty$ to get the desired result. Let C_n be the capacity for one realization of the channel and assume that n belongs to time interval $[0, T]$. For each sub-channel, we define $\beta_n(f_i) = Z_w(f_i) / \left(G(f_i, d)|h_n(f_i)|^2\right)$. We first maximize C_n with respect to the input PSD $P_n(f_i)$, then we average over all realizations of fading states [33]. The objective function C_n is given by

$$C_n = \lim_{N\to\infty} \frac{1}{2N} \sum_{i=1}^{N} \log\left(1 + \frac{P_n(f_i)}{\beta_n(f_i)}\right). \tag{53}$$

The solution involves a combination of water-filling over frequency and time, i.e.,

$$P_{\text{n,opt}}(f_i) = [v_n - \beta_n(f_i)]^+. \tag{54}$$

In the limit of $N \to \infty$, as the number of sub-bands N grows, the width of sub-bands goes to zero and the optimal power allocation converges to

$$P_{\text{n,opt}}(f) = [v_n - \beta_n(f)]^+ \tag{55}$$

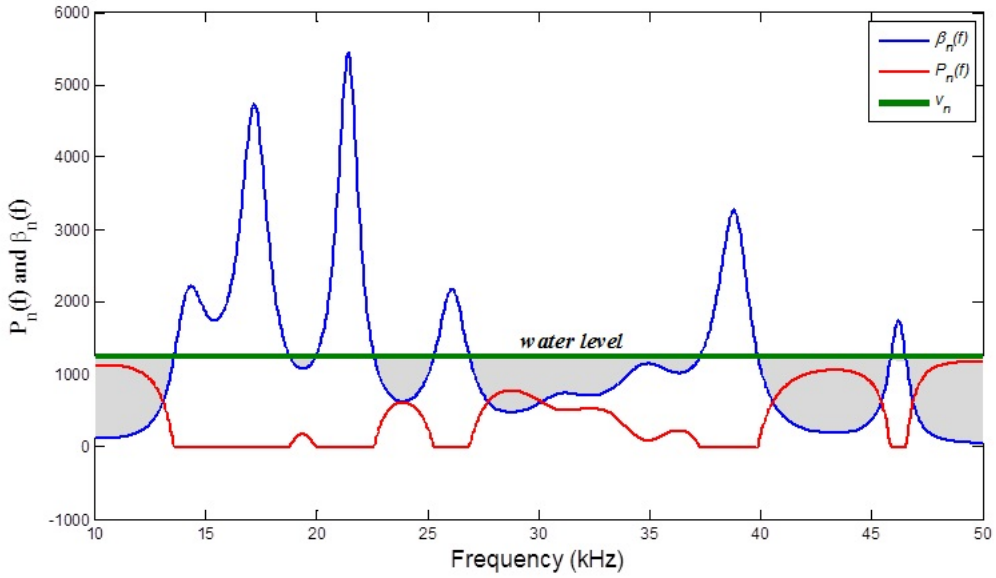

Figure 15: Input power allocation for one realization of the channel ($m = 10$).

where v_n is the power price chosen to satisfy the power constraint for the n^{th} realization of the channel. Considering a defined bandwidth W, we can write

$$\frac{1}{W}\int_{W}\left[v_n - \beta_n\left(f\right)\right]^{+}df = P_t. \tag{56}$$

In Fig. 15, the power allocation procedure for a single realization of the channel is depicted for $f_c = 30$ kHz, $W = 40$ kHz, and $m = 10$. The active regions (i.e., the regions where the power is allocated and is not equal to zero *or* non-zero power regions) are the areas between the solutions of the equation $\beta_n\left(f\right) = v_n$ where $\beta_n\left(f\right) \leq v_n$ (i.e. shaded areas in Fig. 15). This procedure is carried out for all realizations of the channel. By averaging over all realizations of the channel, the optimized capacity is obtained. Fig. 16 depicts results for equal and optimal power allocation. For $d = 1.5$ km, a capacity of 0.77 bits/s/Hz is achieved for equal power allocation. This increases to 0.84 bits/s/Hz for optimal power allocation.

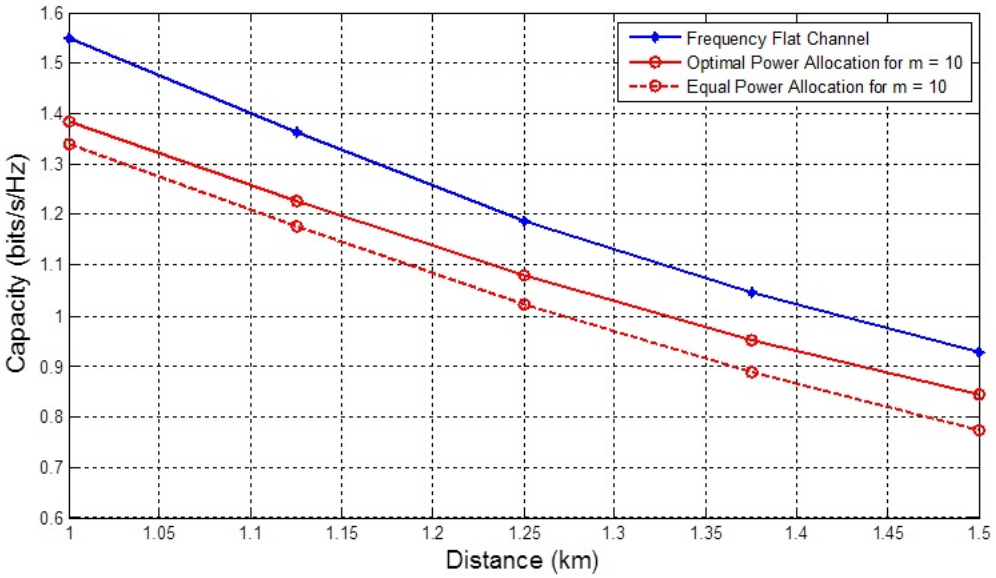

Figure 16: Capacity versus distance for optimal and equal power allocation of input PSD (SNR=10 dB).

3.5.3 Optimal Bandwidth

It is possible to further optimize the capacity in (29) with respect to bandwidth. In order to compare the capacities with different bandwidths in a fair way, neither a pre-specified SNR nor a fixed transmit power is applicable in our case. In UWA communication under consideration, SNR is dependent on the operating frequency band (due to frequency dependency of ambient noise and path loss) and, therefore, to achieve a fixed SNR, either an increase in bandwidth or an increase in transmission power is needed. In both cases, this results in an increase of the total energy of the signal. Likewise, a fixed transmission power P_t is not fair since the larger bandwidths will result in larger capacity as the total energy of the signal (i.e., $P_t W$) increases. Here, we make our comparisons under the assumption of fixed total energy of the signal, i.e., $E_s = P_t W$ and find the optimal bandwidth.

In order to optimize the capacity with respect to bandwidth, we can adopt two different approaches:

- Finding the optimal bandwidth for each realization of the channel,
- Finding a single optimal bandwidth for the average capacity.

The derivations for the first approach can be found in Appendix B. Here, we investigate the second approach which is also of more practical values since most communication systems typically work in a predefined bandwidth region.

The capacity of the Gaussian channel is a concave function of P_t [34], therefore under the assumption of fixed value for E_s, it is also a concave function of W. The optimum value of W, W_{opt}, can be found by iterative methods. The optimized C_n can be then written as

$$C_{\mathrm{n}} = \frac{1}{2} \int\limits_{W_{\mathrm{opt}}} \log\left(1 + \frac{\left[v_n - \beta_n\left(f\right)\right]^+}{\beta_n\left(f\right)}\right) df. \tag{57}$$

The optimal input PSD has a water-filling type structure over both frequency and time and shows a "floating" effect since it changes with respect to time. In order to capture the effect of fading, we need to average C_{n} over time interval $[0, T]$ which is given by $(1/T)\sum_{n=1}^{T} C_{\mathrm{n}}$. As $T \to \infty$ this quantity converges to the expectation by the law of large numbers and can be expressed as

$$C = E_{|h(f)|^2}\left[\frac{1}{2} \int\limits_{W_{\mathrm{opt}}} \log\left(1 + \frac{\left[v - \beta\left(f\right)\right]^+}{\beta\left(f\right)}\right) df\right]. \tag{58}$$

In the following, we assume $d = 350$ m, $T = 22°$C, $D = 50$ m, $S = 35$ ppt and use the corresponding optimal carrier frequency (i.e., $f_{\mathrm{opt}} = 55$ kHz). In Table I, the optimal bandwidth W_{opt} is presented for optimal and equal power allocation.

In Fig. 17, the capacity in bits/s versus different bandwidths is depicted assuming $E_s = 50$, 55, and 60 dB. As we expect from Table 1, the optimized capacity (with respect to bandwidth) takes place at $W_{opt} = 32$, 43, and 55 kHz respectively for $E_s = 50$, 55, and 60 dB under the assumption of equal power allocation. This is

Table 1: Optimal bandwidths obtained for different values of E_s.

E_s (dB)		**10**	**15**	**20**	**25**	**30**	**35**	**40**	**45**	**50**	**55**	**60**	**65**	**70**
W_{opt} (kHz)	Optimal Power Allocation (CSI)	7	10	13	17	22	28	35	44	52	60	68	78	88
	Equal Power Allocation (No CSI)	2	3	4	5	8	12	17	23	32	43	55	69	82

readily confirmed from Fig. 17. The corresponding capacity values are 2.65, 6.85, and 16.21 kbits/s.

As a benchmark, we also calculate the 3dB-bandwidth. This defines the range of frequencies which satisfy

$$\frac{G\left(f,d\right)}{Z_w\left(f\right)} \geq \frac{1}{2}\frac{G\left(f_{\text{opt}},d\right)}{Z_w\left(f_{\text{opt}}\right)}. \tag{59}$$

In our case, the 3dB-bandwidth is obtained as $W_{3dB} = 72.7$ kHz (see Fig. 18). The corresponding capacity values are 5.28, 11.10, and 22.01 kbits/s respectively for $E_s =$ 50, 55, and 60 dB under the assumption of optimal power allocation.

Optimum power allocation along with optimized bandwidth will further increase the capacity. From Fig. 17, we observe that the capacity climbs up to 5.76, 11.47, and 22.11 kbits/s, respectively, for $E_s = 50$, 55, and 60 dB in the case of optimal power allocation. It should be noted that optimal power allocation does not help for the bandwidths larger than the optimal bandwidth. In these cases, capacity remains approximately constant in comparison to the capacity obtained under optimal bandwidth. Since waterfilling prevents the use of excessive bandwidth, increasing the bandwidth is useless. In equal power allocation, when the bandwidth is larger than the optimal bandwidth, capacity is much reduced in comparison to the capacity obtained under optimal bandwidth. The reason is that we allocate the power all over the available bandwidth and energy is now wasted in parts of the channel that should have been turned off because of the low channel quality.

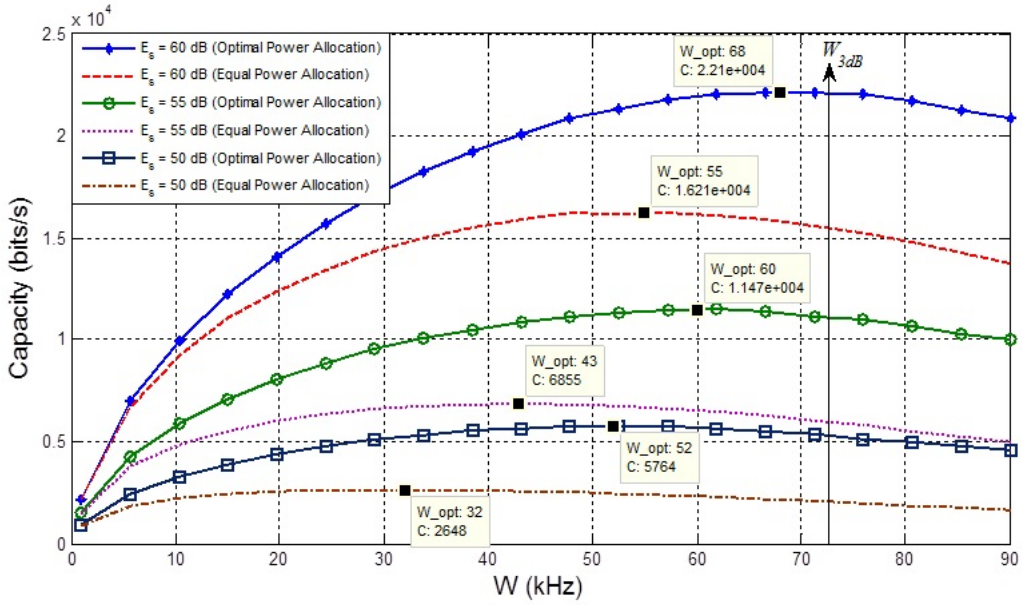

Figure 17: Capacity vs. different values of bandwidth ($d = 350$ m).

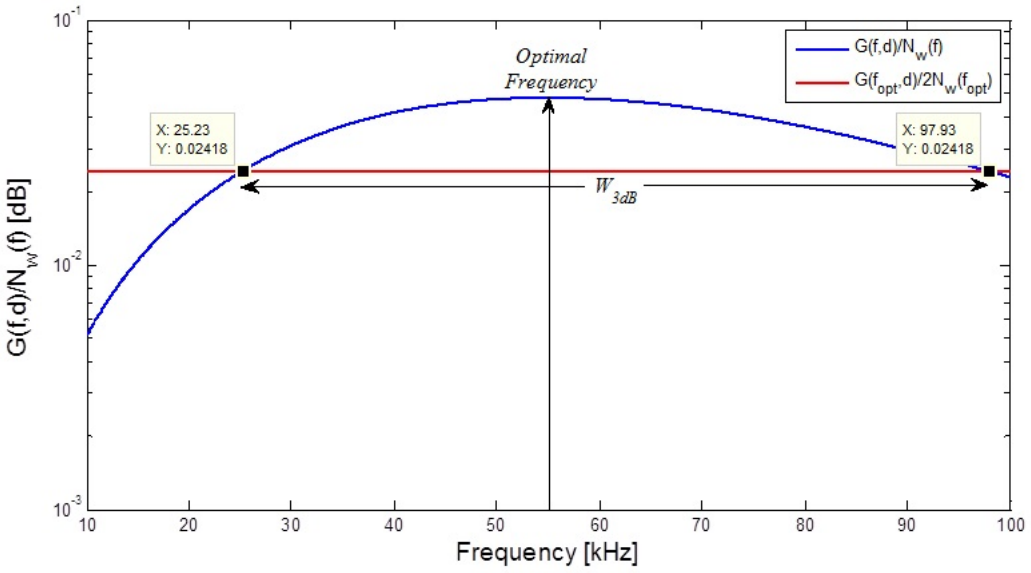

Figure 18: Definition of 3dB bandwidth.

CHAPTER IV

INFORMATION THEORETICAL PERFORMANCE ANALYSIS AND OPTIMIZATION OF RELAY-ASSISTED UWA CHANNELS

Our main objective in this chapter is to determine the fundamental performance bounds on information theoretical limits of single-carrier cooperative UWA communication systems with orthogonal DF relaying. Exploiting the methodology introduced in [27] and [20], we will provide an information theoretic framework for the performance analysis of relay-assisted UWA communication. Specifically, we will derive the UWA channel achievable rates taking into account the effect of relay geometry and determine the achievable maximum rates by optimal input signaling. We will further determine the location of the relay to optimize the achievable rates. Analytical results will be further confirmed through extensive Monte Carlo simulations.

4.1 Transmission Model

We consider a single-relay scenario where nodes are equipped with single transmitter (speaker) and receiver (hydrophone). As illustrated in Fig. 2.b, source (S), relay (R), and destination (D) nodes are assumed to be located in a two-dimensional plane. Our cooperative system builds upon the orthogonal cooperation protocol of [35] (see Fig. 19). In the broadcasting phase, the source transmits the message signals which are received by both the destination and the relay. In the relaying phase, the source is silent and the relay transmits the decoded signal.

We consider a block size of N. Let $x_{S1}[k]$ and $x_R[k]$, $k = 1, 2, \ldots, N$ denote the discrete time signals transmitted by the source during the broadcasting phase

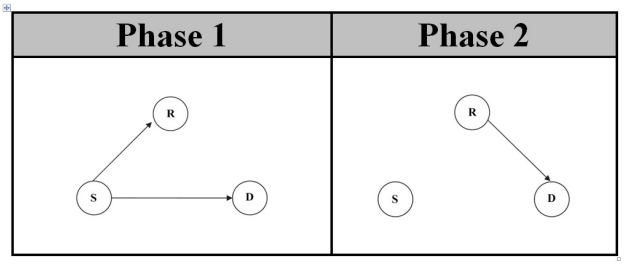

Figure 19: Orthogonal cooperation protocol.

and by the relay during the relaying phase. The autocorrelation function and the corresponding discrete PSD of the input signals are defined as $R_l[k] \overset{F}{\longleftrightarrow} P_l(f_n)$, $k \in \{1, 2, \ldots, N\}$, $l \in \{S_1, R\}$. Let $\mathbf{x}_l = (x_l[1], x_l[2], \ldots, x_l[N])$, $l \in \{S_1, R\}$ denote the transmitted source and relay signals over a block in a vector format. $\mathbf{R}_l = E(\mathbf{x}_l \mathbf{x}_l^*)$ $l \in \{S_1, R\}$ denote the corresponding autocorrelation matrices.

We assume a total transmit power of $2P_T$ during two phases (i.e., broadcasting and relaying) yielding an average power in proportion to P_T per phase. The power constraint during each phase is given by

$$\frac{1}{N}\sum_{k=1}^{N} E\left(|x_{S1}[k]|^2\right) \leq P_{T1} \tag{60}$$

$$\frac{1}{N}\sum_{k=1}^{N} E\left(|x_R[k]|^2\right) \leq P_{T2} \tag{61}$$

where $P_{T1} + P_{T2} = 2P_T$ and $2NP_T$ is the maximum average energy allowed per block. Expectations in (60) and (61) are with respect to the distributions of $\mathbf{x}_l$, i.e., $p(\mathbf{x}_l) = \prod_{i=1}^{N} p(x_l[i]\,|x_l[i-1])$ and $l \in \{S_1, R\}$.

We assume that the relay decodes the received signal correctly and re-transmits after performing a scaling operation to control the transmit power. Mathematically speaking, we define a scaling matrix $\mathbf{V} = \text{diag}\{V_1, V_2, \ldots, V_N\}$ and the transmitted signal by the relay can be represented as $\mathbf{x}_R = \mathbf{V}\mathbf{x}_{S1}$. Consequently, we have $\mathbf{R}_R = \mathbf{V}\mathbf{R}_{S1}\mathbf{V}^*$. Assuming the channel remains unchanged during two phases, the received

signals at the destination and the relay are given by

$$y_R[k] = h_{SR}[k,l] * g_{SR}[k] * x_{S1}[k] + w_R[k], \qquad k = 1, 2, \ldots, N \tag{62a}$$

$$y_{D1}[k] = h_{SD}[k,l] * g_{SD}[k] * x_{S1}[k] + w_{D1}[k], \qquad k = 1, 2, \ldots, N \tag{62b}$$

$$y_{D2}[k] = h_{RD}[k,l] * g_{RD}[k] * x_R[k] + w_{D2}[k], \qquad k = 1, 2, \ldots, N \tag{62c}$$

where $w_l[k]$, $l \in \{D_1, D_2, R\}$ are independent additive non-white Gaussian noise processes with $R_l^w[k] \overset{F}{\longleftrightarrow} Z_w(f_n)$, $k \in \{1, 2, \ldots, N\}$ denoting the autocorrelation function and the corresponding discrete PSD. Note that in the limit of $N \to \infty$, $Z_w(f_n)$ converges to $Z_w(f)$ in (13) by definition of DFT. The autocorrelation matrix of noise signal is defined as $\mathbf{R}_l^w = E(\mathbf{w}_l \mathbf{w}_l^*)$ based on the discrete version of auto-correlation function given by (14). In (62a-c), $g_l[k] \overset{F}{\longleftrightarrow} g_l(f_n)$, $l \in \{SR, SD, RD\}$ $k \in \{1, 2, \ldots, N\}$ represent the effect of large-scale impairments and are discrete versions of function $g_l(t)$ whose PSD is given by the geometrical gains $G_l(f)$, $l \in \{SR, SD, RD\}$ defined in (3-5). We assume a common channel length, L, for the underlying links. Replacing (6) in (62a-c), we have

$$y_R[k] = \sum_{i=1}^{L} h_{SR,i} (g_{SR} * x_{S1})[k-i] + w_R[k], \tag{63a}$$

$$y_{D1}[k] = \sum_{i=1}^{L} h_{SD,i} (g_{SD} * x_{S1})[k-i] + w_{D1}[k], \tag{63b}$$

$$y_{D2}[k] = \sum_{i=1}^{L} h_{RD,i} (g_{RD} * x_R)[k-i] + w_{D2}[k]. \tag{63c}$$

The channels in (62a-c) are referred to as "Linear Gaussian Relay Channel (LGRC)" [20]. In the following, we exploit a technique first introduced in [27] and extended to relay channels in [20]. This technique is based on the development of an *equivalent hypothetical* circular channel model for the N-LGRC channel. This is named as "N-block Circular Gaussian Relay Channel (N-CGRC)" and has been shown to have the same capacity with that of LGRC in the limit of infinite block length [20]. In this

equivalent model, the received signals are given by

$$\bar{y}_R[k] = \sum_{i=1}^{L}\sum_{j=1}^{N} h_{SR,i} g_{SR}[j]\, x_{S1}[(k-i-j)_N] + \bar{w}_R[k] \tag{64a}$$

$$\bar{y}_{D1}[k] = \sum_{i=1}^{L}\sum_{j=1}^{N} h_{SD,i} g_{SD}[j]\, x_{S1}[(k-i-j)_N] + \bar{w}_{D1}[k] \tag{64b}$$

$$\bar{y}_{D2}[k] = \sum_{i=1}^{L}\sum_{j=1}^{N} h_{RD,i} g_{RD}[j]\, x_{R}[(k-i-j)_N] + \bar{w}_{D2}[k] \tag{64c}$$

where the operator $(.)_N$ is defined as

$$(k)_N = \begin{cases} k - N\left\lfloor \frac{k}{N} \right\rfloor & \text{if} \quad k \neq lN,\ l \in \mathbb{Z}_0 \\ N & \text{if} \quad k = lN,\ l \in \mathbb{Z}_0 \end{cases}. \tag{65}$$

Considering the definition of circular convolution, (64a-c) can be rewritten as

$$\bar{y}_R[k] = h_{SR}[k,l] \otimes g_{SR}[k] \otimes x_{S1}[k] + \bar{w}_R[k] \tag{66a}$$

$$\bar{y}_{D1}[k] = h_{SD}[k,l] \otimes g_{SD}[k] \otimes x_{S1}[k] + \bar{w}_{D1}[k] \tag{66b}$$

$$\bar{y}_{D2}[k] = h_{RD}[k,l] \otimes g_{RD}[k] \otimes x_{R}[k] + \bar{w}_{D2}[k]. \tag{66c}$$

In (66a-c), $\bar{w}_l[k]$, $l \in \{D_1, D_2, R\}$ are additive non-white Gaussian noise terms with periodic autocorrelation function [30] given by $E(\bar{w}_l[k]\,\bar{w}_l[j]) = R_l^w[k-j] + R_l^w[k-j+N] + R_l^w[k-j-N]$. Noting that it is a periodic repetition of R_l^w and noise samples from different blocks are independent, we have $R_l^{\bar{w}}[k] = R_l^w[k]$ and $Z_{\bar{w}}(f_n) = Z_w(f_n)$ for $\forall n \in \{1, 2, \ldots, N\}$.

The received signals in (66a-c) can be written in a vector form as

$$\bar{\mathbf{y}}_R = \mathbf{C}_{SR}\mathbf{H}_{SR}\mathbf{x}_{S1} + \bar{\mathbf{w}}_R \tag{67a}$$

$$\bar{\mathbf{y}}_{D1} = \mathbf{C}_{SD}\mathbf{H}_{SD}\mathbf{x}_{S1} + \bar{\mathbf{w}}_{D1} \tag{67b}$$

$$\bar{\mathbf{y}}_{D2} = \mathbf{C}_{RD}\mathbf{H}_{RD}\mathbf{x}_{R} + \bar{\mathbf{w}}_{D2} \tag{67c}$$

where $\bar{\mathbf{y}}_l = (\bar{y}_l[1], \bar{y}_l[2], \ldots, \bar{y}_l[N])$, $\bar{\mathbf{w}}_l = (\bar{w}_l[1], \bar{w}_l[2], \ldots, \bar{w}_l[N])$, $l \in \{D_1, D_2, R\}$. Here, $\mathbf{C}_l$ and $\mathbf{H}_l$, $l \in \{SR, SD, RD\}$ are circulant matrices with elements $[\mathbf{H}_l]_{i,j} =$

$h_{l,(j-i+1)_N}$ and $[\mathbf{C}_l]_{i,j} = g_l[(j-i+1)_N]$. Note that circulant matrices can be diagonalized by DFT matrix $\mathbf{F}$. By taking the DFT of both sides in (67a-c), we have

$$\bar{\mathbf{Y}}_R = \mathbf{G}_{SR}\mathbf{D}_{SR}\mathbf{X}_{S1} + \bar{\mathbf{W}}_R \tag{68}$$

$$\bar{\mathbf{Y}}_{D1} = \mathbf{G}_{SD}\mathbf{D}_{SD}\mathbf{X}_{S1} + \bar{\mathbf{W}}_{D1} \tag{69}$$

$$\bar{\mathbf{Y}}_{D2} = \mathbf{G}_{RD}\mathbf{D}_{RD}\mathbf{X}_R + \bar{\mathbf{W}}_{D2} \tag{70}$$

where $\mathbf{G}_l = \mathbf{F}\mathbf{C}_l\mathbf{F}^*$, $\mathbf{D}_l = \mathbf{F}\mathbf{H}_l\mathbf{F}^*$ for $l \in \{SR, SD, RD\}$, $\bar{\mathbf{Y}}_l = \mathbf{F}\bar{\mathbf{y}}_l$, $\bar{\mathbf{W}}_l = \mathbf{F}\bar{\mathbf{w}}_l$ for $l \in \{D_1, D_2, R\}$, $\mathbf{X}_l = \mathbf{F}\mathbf{x}_l$ for $l \in \{S_1, R\}$ and $\mathbf{X}_R = \bar{\mathbf{V}}\mathbf{X}_{S1}$ with $\bar{\mathbf{V}} = \mathbf{F}\mathbf{V}\mathbf{F}^*$.

Note that $\mathbf{G}_l$ and $\mathbf{D}_l$ are diagonal matrices with diagonal elements $\mathbf{G}_{l,nn} = \sum_{k=1}^{N} g_l[k]\, e^{-j2\pi(k-1)(n-1)/N}\Delta f$ and $\mathbf{D}_{l,nn} = \sum_{i=1}^{L} h_{l,i} e^{-j2\pi(i-1)(n-1)/N}\Delta f$. Equivalently, we have $\mathbf{D}_{l,nn} = h_l(f_n)$ and $\mathbf{G}_{l,nn} = g_l(f_n)$ where $l \in \{SR, SD, RD\}$. The output sequence at the destination node in matrix form is given by

$$\begin{bmatrix} \bar{\mathbf{Y}}_{D1} \\ \bar{\mathbf{Y}}_{D2} \end{bmatrix} = \begin{bmatrix} \mathbf{G}_{SD}\mathbf{D}_{SD} \\ \mathbf{G}_{RD}\mathbf{D}_{RD}\bar{\mathbf{V}} \end{bmatrix} [\mathbf{X}_{S1}] + \begin{bmatrix} \bar{\mathbf{W}}_{D1} \\ \bar{\mathbf{W}}_{D2} \end{bmatrix}. \tag{71}$$

4.2 Derivation of Instantaneous Achievable Rate

Let R denote the transmission rate associated with the signal vector $\mathbf{X}_{S1}$. The equivalent N-CGRC model decomposes the multipath channel into a set of N parallel Gaussian channels via DFT decomposition. The achievable rates of the LGRC under consideration can be then found by letting $N \to \infty$. Considering the input-output relation in (68-70) and noting that the linear DFT operation does not affect the information rate of the channel, R must satisfy [36]

$$R \leq \lim_{N\to\infty} \sup_{P(\mathbf{x}_{S1})} \frac{1}{N} I\left(\bar{\mathbf{Y}}_R; \mathbf{X}_{S1}\right), \tag{72}$$

$$R \leq \lim_{N\to\infty} \sup_{P(\mathbf{x}_{S1})} \frac{1}{N} I\left(\bar{\mathbf{Y}}_{D1}, \bar{\mathbf{Y}}_{D2}; \mathbf{X}_{S1}\right) \tag{73}$$

in order to have successful decoding at the destination terminal. Here, the maximization is taken over the input distribution $P(\mathbf{x}_{S1})$ subject to power constraints. The

transmission rate R must satisfy (72) for an error-free estimate of the transmitted signal at the relay in DF mode.

First, we assume that CSI is present at both transmitter and receiver sides. In order to find the first constraint on R, i.e., (72), we start by defining the mutual information on the right hand side of (72) as

$$I\left(\bar{\mathbf{Y}}_R;\mathbf{X}_{S1}\right)=\mathcal{H}\left(\bar{\mathbf{Y}}_R\right)-\mathcal{H}\left(\bar{\mathbf{Y}}_R|\mathbf{X}_{S1}\right) \tag{74}$$

where $\mathcal{H}\left(.\right)$ is differential entropy. Replacing (68) in (74), we have

$$\begin{aligned} I\left(\bar{\mathbf{Y}}_R;\mathbf{X}_{S1}\right)&=\mathcal{H}\left(\mathbf{G}_{SR}\mathbf{D}_{SR}\mathbf{X}_{S1}+\bar{\mathbf{W}}_R\right)-\mathcal{H}\left(\bar{\mathbf{W}}_R\right)\\ &\leq\frac{1}{2}log2\pi e\left|\mathbf{G}_{SR}\mathbf{D}_{SR}\mathbf{K}_{S1}\mathbf{D}_{SR}^{*}\mathbf{G}_{SR}^{*}+\mathbf{K}_R^{\bar{\mathbf{W}}}\right|-\frac{1}{2}log2\pi e\left|\mathbf{K}_R^{\bar{\mathbf{W}}}\right| \end{aligned} \tag{75}$$

where $\mathbf{K}_{S1}=E\left(\mathbf{X}_{S1}\mathbf{X}_{S1}^{*}\right)=\mathbf{F}\mathbf{R}_{S1}\mathbf{F}^{*}$ and $\mathbf{K}_R^{\bar{\mathbf{W}}}=E\left(\bar{\mathbf{W}}_R\bar{\mathbf{W}}_R^{*}\right)=\mathbf{F}\mathbf{R}_R^{\bar{w}}\mathbf{F}^{*}=\mathbf{F}\mathbf{R}_R^{w}\mathbf{F}^{*}$ are, respectively, DFT of input and relay noise autocorrelation matrices. Due to periodic property of autocorrelation function $R_R^{\bar{w}}\left[k\right]$, the autocorrelation matrix $\mathbf{R}_R^{\bar{w}}$ is circulant. Hence, $\mathbf{R}_R^{\bar{w}}$ can be diagonalized by the DFT matrix $\mathbf{F}$ which results in diagonality of $\mathbf{K}_R^{\bar{\mathbf{W}}}$. The inequality in (75) comes from the fact that Gaussian distribution of input maximizes the entropy.

Hadamard's inequality [31] implies that diagonal $\mathbf{K}_{S1}$ maximizes the mutual information. Therefore, (75) is further upper bounded by

$$I\left(\bar{\mathbf{Y}}_R;\mathbf{X}_{S1}\right)\leq\frac{1}{2}\sum_{n=1}^{N}\ \log\left(1+\frac{\left|\mathbf{G}_{SR}\left[nn\right]\right|^2\left|\mathbf{D}_{SR}\left[nn\right]\right|^2\mathbf{K}_{S1}\left[nn\right]}{\mathbf{K}_R^{\bar{\mathbf{W}}}\left[nn\right]}\right) \tag{76}$$

where $\mathbf{K}_{S1}\left[nn\right]=\sum_{k=1}^{N}R_{S1}\left[k\right]e^{-j2\pi(k-1)(n-1)/N}\Delta f$ and $\mathbf{K}_R^{\bar{\mathbf{W}}}\left[nn\right]=\sum_{k=1}^{N}R_R^{\bar{w}}\left[k\right]e^{-j2\pi(k-1)(n-1)/N}\Delta f$ are respectively the diagonal components of $\mathbf{K}_{S1}$ and $\mathbf{K}_R^{\bar{\mathbf{W}}}$. These correspond to the discrete values of input PSD and noise PSD evaluated at the n'th frequency bin f_n, i.e., $\mathbf{K}_{S1}\left[nn\right]=P_{S1}\left(f_n\right)$, $\mathbf{K}_R^{\bar{\mathbf{W}}}\left[nn\right]=Z_w\left(f_n\right)$. In (76), we replace $\left|\mathbf{G}_{SR}\left[nn\right]\right|^2$ and $\left|\mathbf{D}_{SR}\left[nn\right]\right|^2$ with $G_{SR}\left(f_n\right)$ and $\left|h_{SR}\left(f_n\right)\right|^2$ respectively. Using the resulting expression,

we can rewrite (72) as

$$R \leq \lim_{N\to\infty} \max_{P_{S1}(f_n)} \frac{1}{2N} \sum_{n=1}^{N} \log\left(1 + \frac{G_{SR}\left(f_n\right)\left|h_{SR}\left(f_n\right)\right|^2 P_{S1}\left(f_n\right)}{Z_w\left(f_n\right)}\right). \tag{77}$$

In the limit of $N \to \infty$, as the number of sub-bands N grows, the frequency width W/N of the sub-bands goes to zero and they represent a sampling of the continuous spectrum. Then (77) converges to

$$R \leq \max_{P_{S1}(f)} \frac{1}{2} \int_{W} \log\left(1 + \frac{G_{SR}\left(f\right)\left|h_{SR}\left(f\right)\right|^2 P_{S1}\left(f\right)}{Z_w\left(f\right)}\right) df \tag{78}$$

where the integration is over the operating band W. In the following, we define $\beta_{SR}\left(f\right) = Z_w\left(f\right) / \left(G_{SR}(f)|h_{SR}(f)|^2\right)$ for the sake of presentation simplicity. This lets us rewrite (78) as

$$R \leq \max_{P_{S1}(f)} \frac{1}{2} \int_{W} \log\left(1 + \frac{P_{S1}\left(f\right)}{\beta_{SR}\left(f\right)}\right) df. \tag{79}$$

In order to find the second constraint on R, i.e (73), we start by defining the mutual information in (73) as

$$I\left(\bar{\mathbf{Y}}_{D1}, \bar{\mathbf{Y}}_{D2}; \mathbf{X}_{S1}\right) = \mathcal{H}\left(\bar{\mathbf{Y}}_{D1}, \bar{\mathbf{Y}}_{D2}\right) - \mathcal{H}\left(\bar{\mathbf{Y}}_{D1}, \bar{\mathbf{Y}}_{D2} | \mathbf{X}_{S1}\right). \tag{80}$$

Replacing (71) in (80), we have

$$\begin{aligned} I\left(\bar{\mathbf{Y}}_{D1}, \bar{\mathbf{Y}}_{D2}; \mathbf{X}_{S1}\right) &= \mathcal{H}\left(\mathbf{G}_{SD}\mathbf{D}_{SD}\mathbf{X}_{S1} + \bar{\mathbf{W}}_{D1}, \mathbf{G}_{RD}\mathbf{D}_{RD}\bar{\mathbf{V}}\mathbf{X}_{S1} + \bar{\mathbf{W}}_{D2}\right) - \mathcal{H}\left(\bar{\mathbf{W}}_{D1}, \bar{\mathbf{W}}_{D2}\right) \\ &\leq \frac{1}{2} log 2\pi e \left| \begin{bmatrix} \mathbf{G}_{SD}\mathbf{D}_{SD}\mathbf{K}_{S1}\mathbf{D}_{SD}^{*}\mathbf{G}_{SD}^{*} & \mathbf{G}_{SD}\mathbf{D}_{SD}\mathbf{K}_{S1}\bar{\mathbf{V}}^{*}\mathbf{D}_{RD}^{*}\mathbf{G}_{RD}^{*} \\ \mathbf{G}_{RD}\mathbf{D}_{RD}\bar{\mathbf{V}}\mathbf{K}_{S1}\mathbf{D}_{SD}^{*}\mathbf{G}_{SD}^{*} & \mathbf{G}_{RD}\mathbf{D}_{RD}\bar{\mathbf{V}}\mathbf{K}_{S1}\bar{\mathbf{V}}^{*}\mathbf{D}_{RD}^{*}\mathbf{G}_{RD}^{*} \end{bmatrix} + \begin{bmatrix} \mathbf{K}_{D1}^{\bar{\mathbf{W}}} & 0 \\ 0 & \mathbf{K}_{D2}^{\bar{\mathbf{W}}} \end{bmatrix} \right| \\ &- \frac{1}{2} log 2\pi e \left| \begin{bmatrix} \mathbf{K}_{D1}^{\bar{\mathbf{W}}} & 0 \\ 0 & \mathbf{K}_{D2}^{\bar{\mathbf{W}}} \end{bmatrix} \right| \end{aligned} \tag{81}$$

where $\mathbf{K}_{l}^{\bar{\mathbf{W}}} = E\left(\bar{\mathbf{W}}_{l}\bar{\mathbf{W}}_{l}^{*}\right) = \mathbf{F}\mathbf{R}_{l}^{\bar{w}}\mathbf{F}^{*} = \mathbf{F}\mathbf{R}_{l}^{w}\mathbf{F}^{*}$, $l \in \{D_1, D_2\}$ are DFT of noise autocorrelation matrices at the destination. Note that $\mathbf{K}_{l}^{\bar{\mathbf{W}}}$ is diagonal, since noise autocorrelation matrix $\mathbf{R}_{l}^{\bar{w}}$ is circulant. The inequality in (81) comes from the fact

that Gaussian input distribution maximizes the entropy. Diagonal $\mathbf{K}_{S1}$ maximizes the mutual information and (81) can be further upper bounded as

$$I\left(\bar{\mathbf{Y}}_{D1},\bar{\mathbf{Y}}_{D2};\mathbf{X}_{S1}\right)\leq\frac{1}{2}\sum_{n=1}^{N}\log\left(1+\frac{\left|\mathbf{G}_{SD}\left[nn\right]\right|^{2}\left|\mathbf{D}_{SD}\left[nn\right]\right|^{2}\mathbf{K}_{S1}\left[nn\right]}{\mathbf{K}_{D1}^{\bar{\mathbf{W}}}\left[nn\right]}\right.$$
$$\left.+\frac{\left|\mathbf{G}_{RD}\left[nn\right]\right|^{2}\left|\mathbf{D}_{RD}\left[nn\right]\right|^{2}\left|\bar{\mathbf{V}}\left[nn\right]\right|^{2}\mathbf{K}_{S1}\left[nn\right]}{\mathbf{K}_{D2}^{\bar{\mathbf{W}}}\left[nn\right]}\right)\quad(82)$$

where $\mathbf{K}_{D1}^{\bar{\mathbf{W}}}\left[nn\right]=\mathbf{K}_{D2}^{\bar{\mathbf{W}}}\left[nn\right]=Z_{w}\left(f_{n}\right)$. Considering $V_{i}\overset{F}{\longleftrightarrow}V(f_{n})$, it can be easily found that $\left|\bar{\mathbf{V}}\left[nn\right]\right|^{2}$ is equivalent to $V\left(f_{n}\right)$. In (82), we replace $\left|\mathbf{G}_{SD}\left[nn\right]\right|^{2}$, $\left|\mathbf{D}_{SD}\left[nn\right]\right|^{2}$, $\left|\mathbf{G}_{RD}\left[nn\right]\right|^{2}$, and $\left|\mathbf{D}_{RD}\left[nn\right]\right|^{2}$ respectively with $G_{SD}\left(f_{n}\right)$, $\left|h_{SD}\left(f_{n}\right)\right|^{2}$, $G_{RD}\left(f_{n}\right)$, and $\left|h_{RD}\left(f_{n}\right)\right|^{2}$. Therefore, we have

$$R\leq\lim_{N\to\infty}\max_{\substack{P_{l}(f_{n})\\l\in\{S1,R\}}}\frac{1}{2N}\sum_{n=1}^{N}\log\left(1+\left[\frac{G_{SD}\left(f_{n}\right)\left|h_{SD}\left(f_{n}\right)\right|^{2}}{Z_{w}\left(f_{n}\right)}\right.\right.$$
$$\left.\left.+\frac{G_{RD}\left(f_{n}\right)\left|h_{RD}\left(f_{n}\right)\right|^{2}V\left(f_{n}\right)}{Z_{w}\left(f_{n}\right)}\right]P_{S1}\left(f_{n}\right)\right).\quad(83)$$

In the limit of $N\to\infty$, (83) converges to

$$R\leq\max_{\substack{P_{l}(f)\\l\in\{S1,R\}}}\frac{1}{2}\int_{W}\log\left(1+\left[\frac{G_{SD}\left(f\right)\left|h_{SD}\left(f\right)\right|^{2}}{Z_{w}\left(f\right)}\right.\right.$$
$$\left.\left.+\frac{G_{RD}\left(f\right)\left|h_{RD}\left(f\right)\right|^{2}V\left(f\right)}{Z_{w}\left(f\right)}\right]P_{S1}\left(f\right)\right)df\quad(84)$$

where the integration is over the operating band. Further defining $\beta_{SD}\left(f\right)=Z_{w}\left(f\right)/\left(G_{SD}(f)|h_{SD}(f)|^{2}\right)$ and $\beta_{RD}\left(f\right)=Z_{w}\left(f\right)/\left(G_{RD}(f)|h_{RD}(f)|^{2}\right)$ for the sake of presentation simplicity, (84) can be written as

$$R\leq\max_{\substack{P_{l}(f)\\l\in\{S1,R\}}}\frac{1}{2}\int_{W}\log\left(1+\frac{P_{S1}\left(f\right)}{\beta_{SD}\left(f\right)}+\frac{V\left(f\right)P_{S1}\left(f\right)}{\beta_{RD}\left(f\right)}\right)df.\quad(85)$$

Recall from (60) and (61) that the maximization of R is subject to power constraints. In the limit of infinite block length ($N \to \infty$), we can rewrite these

$$\frac{1}{W}\int_{W} P_{S1}(f)\,df \leq P_T$$
$$\frac{1}{W}\int_{W} P_{R}(f)\,df \leq P_T$$

If CSI is not available at the transmitter, total power is distributed equally between the source and relay. In the case of equal power allocation, input powers are set as $P_{S1}(f) = P_T$, $P_R(f) = P_T$ and the associated overall achievable rate of the channel is therefore obtained as

$$R = \frac{1}{4}\min\left\{\int_{W}\log\left(1+\frac{P_T}{\beta_{SR}(f)}\right)df, \int_{W}\log\left(1+\frac{P_T}{\beta_{SD}(f)}+\frac{P_T}{\beta_{RD}(f)}\right)df\right\}. \quad (86)$$

Note that achievable rate is divided by two, because the transmission of a symbol requires two time slots.

4.3 Derivation of Average Achievable Rate

The expression in (86) has been obtained for a given realization of the channel. To find the average capacity, one needs to take expectation of (86) with respect to distribution of $|h_l(f)|^2$, $l \in \{SR, SD, RD\}$. $h_l(f)$ is the Fourier Transform of the discrete channel taps, i.e., $h_l(f) = \sum_{i=1}^{L} h_{l,i} e^{-j2\pi f(i-1)}$ where $h_{l,i}$'s are complex Gaussian random processes with independent real and imaginary parts having a mean of $\mu_{l,i}/\sqrt{2}$ and a variance of $\sigma_{l,i}^2$ (c.f. Section 2.2). Since $h_l(f)$ is a linear summation of independent complex Gaussian random processes, it is also a complex Gaussian random process with mean $\mu_l(f) = \sum_{i=1}^{L} E(h_{l,i})\, e^{-j2\pi f(i-1)}$ and variance $\sigma_l^2 = \sum_{i=1}^{L} 2\sigma_{l,i}^2$. It is therefore easy to see that $|h_l(f)|^2$follows the exponential pdf given by [32]

$$p\left(|h_l(f)|^2\right) = \frac{1}{1+\lambda_l}\exp\left(-\frac{|h_l(f)|^2}{1+\lambda_l}\right) \quad (87)$$

where $\lambda_l = 2\sum_{i=1}^{L}\sum_{j=i+1}^{L}\mu_{l,i}\mu_{l,j}\cos(2\pi f(j-i))$and $l \in \{SR, SD, RD\}$.

To find the average achievable rate, we need to calculate

$$\bar{R} = E_{|h_l(f)|^2}\left(\frac{1}{4}\min\left\{\int_W \log\left(1+\frac{P_T}{\beta_{SR}(f)}\right)df, \int_W \log\left(1+\frac{P_T}{\beta_{SD}(f)}+\frac{P_T}{\beta_{RD}(f)}\right)df\right\}\right). \quad (88)$$

Replacing $\beta_{SR}(f)$ in (88), we rewrite the first limiting expression in (88) as

$$\bar{R}_1 = E_{|h_{SR}(f)|^2}\left(\frac{1}{4}\int_W \log\left(1+\frac{G_{SR}(f)P_T}{Z_w(f)}|h_{SR}(f)|^2\right)df\right). \quad (89)$$

Here, we need to take an expectation with respect to $|h_{SR}(f)|^2$ which has an exponential PDF given by (87). Defining $\rho = |h_{SR}(f)|^2/(1+\lambda_{SR})$, (89) can be written as

$$\bar{R}_1 = \frac{1}{4}\int_W \int_0^\infty \log\left(1+\frac{(1+\lambda_{SR})G_{SR}(f)P_T}{Z_w(f)}\rho\right)\exp(-\rho)d\rho df. \quad (90)$$

Defining the integral $\mathcal{I}_n(x)$ as

$$\mathcal{I}_n(x) = \int_0^\infty t^{n-1}\ln(1+t)e^{-xt}dt; \qquad x>0, \qquad n=1,2,... \quad (91)$$

we can rewrite (90) as

$$\bar{R}_1 = \frac{\log_2(e)}{4}\int_W \left(\frac{Z_w(f)}{(1+\lambda_{SR})G_{SR}(f)P_T}\right)\mathcal{I}_1\left(\frac{Z_w(f)}{(1+\lambda_{SR})G_{SR}(f)P_T}\right)df. \quad (92)$$

Using the results of [32], we can write

$$\bar{R}_1 = \frac{\log_2(e)}{4}\int_W \exp\left(\frac{Z_w(f)}{(1+\lambda_{SR})G_{SR}(f)P_T}\right)\Gamma\left(0,\frac{Z_w(f)}{(1+\lambda_{SR})G_{SR}(f)P_T}\right)df \quad (93)$$

where $\Gamma(a,z) = \int_z^\infty t^{a-1}e^{-t}dt$ denotes the *incomplementary gamma function* [32]. Using the first series expansion of $\Gamma(0,z)$ [32,33] and substituting it in (93), we have

$$\bar{R}_1 = \frac{\log_2(e)}{4}\int_W \exp\left(\frac{Z_w(f)}{(1+\lambda_{SR})G_{SR}(f)P_T}\right)\left[-\gamma+\ln\left(\frac{(1+\lambda_{SR})G_{SR}(f)P_T}{Z_w(f)}\right)\right.$$
$$\left.-\sum_{k=1}^\infty \frac{1}{k.k!}\left(\frac{-Z_w(f)}{(1+\lambda_{SR})G_{SR}(f)P_T}\right)^k\right]df \quad (94)$$

where γ is the Euler constant ($\gamma = 0.577215665$). At high SNR values, (94) can be approximated as

$$\bar{R}_1 \simeq \frac{\log_2(e)}{4} \int\limits_W \exp\left(\frac{Z_w(f)}{(1+\lambda_{SR})\, G_{SR}(f)\, P_T}\right) \left[-\gamma + \ln\left(\frac{(1+\lambda_{SR})\, G_{SR}(f)\, P_T}{Z_w(f)}\right) + \frac{Z_w(f)}{(1+\lambda_{SR})\, G_{SR}(f)\, P_T}\right] df. \tag{95}$$

Replacing $\beta_{SD}(f)$ and $\beta_{RD}(f)$ in (88), we rewrite the second limiting expression in (88) as

$$\bar{R}_2 = E_{\text{joint}}\left(\frac{1}{4}\int\limits_W \log\left(1 + \frac{G_{SD}(f)\, P_T}{Z_w(f)}|h_{SD}(f)|^2 + \frac{G_{RD}(f)\, P_T}{Z_w(f)}|h_{RD}(f)|^2\right) df\right) \tag{96}$$

where the expectation is with respect to the joint distribution of $|h_{SD}(f)|^2$ and $|h_{RD}(f)|^2$. Note that $|h_{SD}(f)|^2$ and $|h_{RD}(f)|^2$ are independent and identical distributed (iid) with exponential distribution. Let us define $\rho_1 = |h_{SD}(f)|^2/(1+\lambda_{SD})$, $\rho_2 = |h_{RD}(f)|^2/(1+\lambda_{RD})$, $b_1 = Z_w(f)/[(1+\lambda_{SD})\, G_{SD}(f)\, P_T]$, and $b_2 = Z_w(f)/[(1+\lambda_{RD})\, G_{RD}(f)\, P_T]$. We can therefore rewrite (96) as

$$\bar{R}_2 = \frac{\log_2(e)}{4} \int\limits_W \int\limits_0^\infty \int\limits_0^\infty \ln\left(1 + \frac{\rho_1}{b_1} + \frac{\rho_2}{b_2}\right) e^{-(\rho_1+\rho_2)} d\rho_1 d\rho_2 df. \tag{97}$$

First we investigate the integration over ρ_1. Using the integration by parts technique, it can be simplified as

$$\int\limits_0^\infty \ln\left(1 + \frac{\rho_1}{b_1} + \frac{\rho_2}{b_2}\right) e^{-\rho_1} d\rho_1 = \ln\left(1 + \frac{\rho_2}{b_2}\right) + \int\limits_0^\infty \frac{e^{-\rho_1}}{b_1(1+\rho_2/b_2) + \rho_1} d\rho_1 \tag{98}$$

where the right hand side integration can be expressed in terms of complementary gamma function by changing the variable of integration. This yields

$$\int\limits_0^\infty \ln\left(1 + \frac{\rho_1}{b_1} + \frac{\rho_2}{b_2}\right) e^{-\rho_1} d\rho_1 = \ln\left(1 + \frac{\rho_2}{b_2}\right) + e^{b_1(1+\rho_2/b_2)}\Gamma\left(0, b_1(1+\rho_2/b_2)\right). \tag{99}$$

Now we perform the integration over ρ_2. This yields

$$\int_0^\infty \int_0^\infty \ln\left(1+\frac{\rho_1}{b_1}+\frac{\rho_2}{b_2}\right) e^{-\rho_1} d\rho_1 e^{-\rho_2} d\rho_2$$

$$= \int_0^\infty \ln\left(1+\frac{\rho_2}{b_2}\right) e^{-\rho_2} d\rho_2 + \int_0^\infty e^{\left(b_1+\frac{b_1-b_2}{b_2}\rho_2\right)} \Gamma\left(0, b_1\left(1+\rho_2/b_2\right)\right) d\rho_2 \tag{100}$$

$$= e^{b_2}\Gamma\left(0,b_2\right) + \frac{b_2 e^{b_2}}{b_1} \int_{b_1}^\infty e^{\left(\frac{b_1-b_2}{b_1}t\right)} \Gamma\left(0,t\right) dt \tag{101}$$

where we define $t = b_1\left(1+\rho_2/b_2\right)$. Assuming $b_1 \neq b_2$ and by using the integration by parts technique, (101) can be expressed as

$$\int_0^\infty \int_0^\infty \ln\left(1+\frac{\rho_1}{b_1}+\frac{\rho_2}{b_2}\right) e^{-\rho_1} d\rho_1 e^{-\rho_2} d\rho_2 \tag{102}$$

$$= e^{b_2}\Gamma\left(0,b_2\right) + \frac{b_2 e^{b_2}}{b_1}\left(\frac{b_1}{b_2-b_1} e^{(b_1-b_2)}\Gamma\left(0,b_1\right) + \frac{b_1}{b_2-b_1}\int_{b_1}^\infty e^{\left(\frac{b_1-b_2}{b_1}t\right)} \frac{\partial\Gamma\left(0,t\right)}{\partial t} dt\right).$$

Noting $\partial\Gamma\left(0,t\right)/\partial t = -t^{-1}e^{-t}$ and replacing it in (102), we have

$$\int_0^\infty \int_0^\infty \ln\left(1+\frac{\rho_1}{b_1}+\frac{\rho_2}{b_2}\right) e^{-\rho_1} d\rho_1 e^{-\rho_2} d\rho_2$$

$$= e^{b_2}\Gamma\left(0,b_2\right) + \frac{b_2 e^{b_2}}{b_2-b_1}\left(e^{(b_1-b_2)}\Gamma\left(0,b_1\right) - \int_{b_1}^\infty e^{\left(-\frac{b_2}{b_1}t\right)} t^{-1} dt\right). \tag{103}$$

Defining $u = \left(b_2/b_1\right)t$, we change the variable of integration at the right hand side of (103) and the integration becomes an incomplementary gamma function. Therefore, we have

$$\int_0^\infty \int_0^\infty \ln\left(1+\frac{\rho_1}{b_1}+\frac{\rho_2}{b_2}\right) e^{-\rho_1} d\rho_1 e^{-\rho_2} d\rho_2$$

$$= e^{b_2}\Gamma\left(0,b_2\right) + \frac{b_2 e^{b_2}}{b_2-b_1}\left(e^{(b_1-b_2)}\Gamma\left(0,b_1\right) - \Gamma\left(0,b_2\right)\right) \tag{104}$$

which can be also rewritten as

$$\int_0^\infty \int_0^\infty \ln\left(1+\frac{\rho_1}{b_1}+\frac{\rho_2}{b_2}\right) e^{-(\rho_1+\rho_2)} d\rho_1 d\rho_2 = \frac{b_2}{b_2-b_1} e^{b_1}\Gamma\left(0,b_1\right) + \frac{b_1}{b_1-b_2} e^{b_2}\Gamma\left(0,b_2\right). \tag{105}$$

Note that for solving the integration in (101), we assumed $b_1 \neq b_2$ which is equivalent to $d_{SD} \neq d_{RD}$. Considering $b_1 = b_2 = b$ (i.e. $d_{SD} = d_{RD}$), the integration in (101) becomes

$$\int_0^\infty \int_0^\infty \ln\left(1+\frac{\rho_1}{b_1}+\frac{\rho_2}{b_2}\right) e^{-\rho_1} d\rho_1 e^{-\rho_2} d\rho_2 = e^b \Gamma(0,b) + e^b \int_b^\infty \Gamma(0,t)\, dt$$
$$= e^b \Gamma(0,b) + e^b \left(\Gamma(1,b) - b\Gamma(0,b)\right). \quad (106)$$

Replacing $\Gamma(1,b) = \exp(-b)$ in (106) yields

$$\int_0^\infty \int_0^\infty \ln\left(1+\frac{\rho_1}{b}+\frac{\rho_2}{b}\right) e^{-(\rho_1+\rho_2)} d\rho_1 d\rho_2 = 1 + (1-b)\, e^b \Gamma(0,b). \quad (107)$$

The average rate can be found by replacing (105) or (107) in (97) which yields the final form as

$$\bar{R}_2 = \begin{cases} \frac{\log_2(e)}{4} \int\limits_W \left[\frac{b_2}{b_2-b_1} e^{b_1}\Gamma(0,b_1) + \frac{b_1}{b_1-b_2} e^{b_2}\Gamma(0,b_2)\right] df & \text{for} \quad d_{SD} \neq d_{RD} \\ \frac{\log_2(e)}{4} \int\limits_W \left[1 + (1-b)\, e^b \Gamma(0,b)\right] df & \text{for} \quad d_{SD} = d_{RD} \end{cases}. \quad (108)$$

where $b_1 = Z_w(f) / [(1+\lambda_{SD}) G_{SD}(f) P_T]$ and $b_2 = Z_w(f) / [(1+\lambda_{RD}) G_{RD}(f) P_T]$. The gamma functions in (108) at high SNR values can be approximated as $\Gamma(0,b) = -\gamma - \ln(b) + b$.

Finally, the average achievable rate is found as

$$\bar{R} = \min\left\{\bar{R}_1, \bar{R}_2\right\} \quad (109)$$

where $\bar{R}_1$ and $\bar{R}_2$ are, respectively, given by (94) and (108). In an effort to demonstrate the accuracy of derived expressions for average channel achievable rate, we plot the derived expressions $\bar{R}_1$, $\bar{R}_2$ in Fig. 20 and compare them with the numerical evaluation of the limiting expressions in (88).

In this figure, we assume $d_h = 0.5$ km, $d_r = 0.5$ km, $f_c = 30$ kHz, $W = 40$ kHz, temperature $T = 22°$C, depth $D = 50$ m, acidity of 8 pH, salinity $S = 35$ ppt, wind speed $\omega = 0$ m/s and spreading factor $s = 1.5$. We assume that the UWA channel

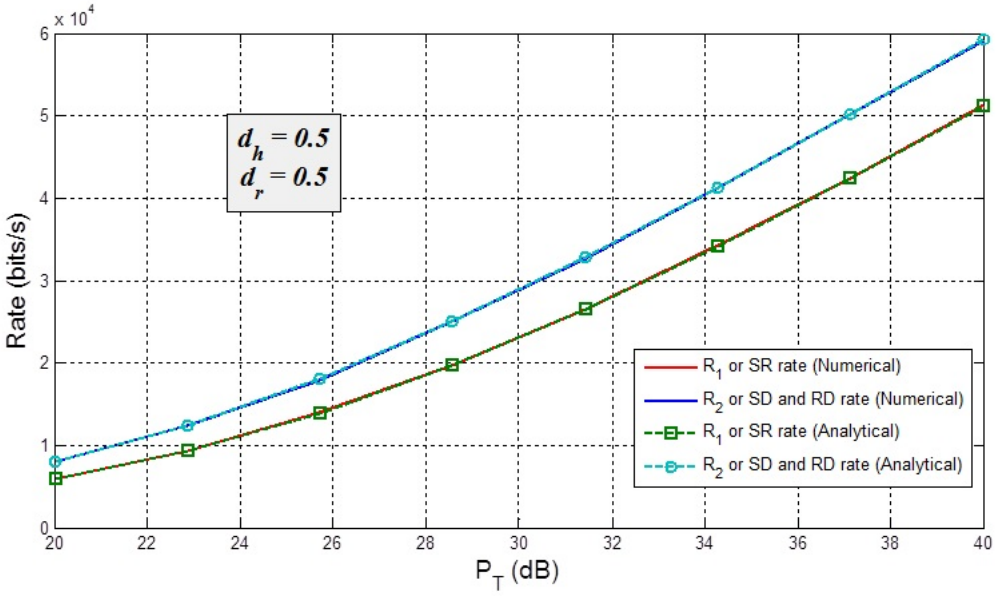

Figure 20: Comparison of derived expressions of average channel achievable rate vs. numerical results.

experiences a multipath delay spread of 13 ms and has the order of $L = 130$. The number of significant delay taps is $m = 10$ and located at equal distances from each other with a uniform PDP. It is observed from Fig. 20 that the derived expressions (94) and (108) coincide perfectly with numerical results. Furthermore, approximated formulas of (94) and (108) obtained by replacing $\Gamma(0, b) \simeq -\gamma - \ln(b) + b$ provide efficient approximations for high SNR values.

4.4 Optimization of the Average Achievable Rate

In the following, we will maximize the average achievable rate through optimal power allocation and relay location under the assumption that CSI is present at both transmitter and receiver side.

4.4.1 Optimal Power Allocation

A direct maximization of (79) and (85) appears to be intractable. We consider the power allocation problem in the continuous frequency domain via discrete frequency domain. We then take the limit as $N \to \infty$ to get the desired result. Therefore, we

formulate our problem as

$$\max_{P_{S1}(f_n)} \min \left\{ \sum_{n=1}^{N} \log \left(1 + \frac{P_{S1}(f_n)}{\beta_{SR}(f_n)} \right), \sum_{n=1}^{N} \log \left(1 + \frac{P_{S1}(f_n)}{\beta_{SD}(f_n)} + \frac{V(f_n) P_{S1}(f_n)}{\beta_{RD}(f_n)} \right) \right\}. \quad (110)$$

We use Lemma 6 of [20] which further simplifies the N-dimensional optimization problem into N parallel optimization problems corresponding to each of the frequency sub bands. For further simplification, we define

$$R_1(f_n) = \log \left(1 + \frac{P_{S1}(f_n)}{\beta_{SR}(f_n)} \right) \quad (111)$$

$$R_2(f_n) = \log \left(1 + \frac{P_{S1}(f_n)}{\beta_{SD}(f_n)} + \frac{V(f_n) P_{S1}(f_n)}{\beta_{RD}(f_n)} \right). \quad (112)$$

Therefore, the aforementioned lemma reduces the original problem into the form of

$$\max_{P_{S1}(f_n)} \min \{ R_1(f_n), R_2(f_n) \}. \quad (113)$$

First, we assume a non-degraded channel [31] where $\beta_{SR}(f_n) \geq \beta_{SD}(f_n)$ for $\forall n$. In this case we have $R_1(f_n) \leq R_2(f_n)$. Therefore, the problem reduces to

$$\max_{P_{S1}(f_n)} \sum_{n=1}^{N} \log \left(1 + \frac{P_{S1}(f_n)}{\beta_{SR}(f_n)} \right). \quad (114)$$

We observe that the resultant solution will be of a water-filling form, i.e., $P_{\mathrm{S1,opt}}(f_n) = [v_t - \beta_{SR}(f_n)]^+$ and $P_{\mathrm{R,opt}}(f_n) = 0$. If the quality of the $(S \to R)$ link is poor, it is better to not allocate any power to the relay and just using the direct link is preferred. However, if the relay is not involved in transmission, the optimal strategy is to transmit with full power of $2P_T$ during the first phase and allocate power with respect to $\beta_{SD}(f_n)$, i.e. $P_{\mathrm{S1,opt}}(f_n) = [v_t - \beta_{SD}(f_n)]^+$ where v_t is the power price chosen to satisfy the overall total input power constraint, i.e.,

$$\frac{1}{N} \sum_{n=1}^{N} [v_t - \beta_{SD}(f_n)]^+ = 2P_T. \quad (115)$$

Second, we assume a degraded channel where $\beta_{SR}(f_n) \leq \beta_{SD}(f_n)$ for $\forall n$. In this case the sub-channel rate is maximized when $R_1(f_n) = R_2(f_n)$ [20] or equivalently

$$\frac{P_{S1}(f_n)}{\beta_{SR}(f_n)} = \frac{P_{S1}(f_n)}{\beta_{SD}(f_n)} + \frac{V(f_n) P_{S1}(f_n)}{\beta_{RD}(f_n)}. \quad (116)$$

From (116), $V(f_n)$ can be found as

$$V(f_n) = \beta_{RD}(f_n)\left(\frac{1}{\beta_{SR}(f_n)} - \frac{1}{\beta_{SD}(f_n)}\right). \tag{117}$$

Again $P_{S1}(f_n)$ has a waterfilling form as $P_{\text{S1,opt}}(f_n) = [v_t - \beta_{SR}(f_n)]^+$ and $P_R(f_n)$ is given by

$$P_{\text{R-opt}}(f_n) = \beta_{RD}(f_n)\left(\frac{1}{\beta_{SR}(f_n)} - \frac{1}{\beta_{SD}(f_n)}\right)[v_t - \beta_{SR}(f_n)]^+ \tag{118}$$

where v_t is the power price chosen to satisfy the overall total input power constraint, i.e.,

$$\frac{1}{N}\sum_{n=1}^{N}\left[1 + \beta_{RD}(f_n)\left(\frac{1}{\beta_{SR}(f_n)} - \frac{1}{\beta_{SD}(f_n)}\right)\right][v_t - \beta_{SR}(f_n)]^+ = 2P_T. \tag{119}$$

Finally, we can find the solution in continuous domain by letting $N \to \infty$.

4.4.2 Optimal Relay Location

First, we replace (3-5) in (78) and (84) and express them in terms of d_h and d_r. Assuming $\bar{R} = \min\left\{\bar{R}_1, \bar{R}_2\right\}$, we will have

$$\bar{R}_1 = E\left(\frac{1}{4}\int_W \log\left(1 + \frac{|h_{SR}(f)|^2 P_{S1}(f)}{Z_w(f)\left(d_h^2 + d_r^2\right)^{s/2} a(f)^{\sqrt{d_h^2+d_r^2}}}\right)df\right) \tag{120}$$

$$\bar{R}_2 = E\left(\frac{1}{4}\int_W \log\left(1 + \left[\frac{|h_{SD}(f)|^2}{Z_w(f)\, d_{SD}^s a(f)^{d_{SD}}} + \frac{|h_{RD}(f)|^2 V(f)}{Z_w(f)\left(d_h^2 + (d_{SD}-d_r)^2\right)^{s/2} a(f)^{\sqrt{d_h^2+(d_{SD}-d_r)^2}}}\right] P_{S1}(f)\right)df\right). \tag{121}$$

In order to maximize $\bar{R}_1$ and $\bar{R}_2$ with respect to d_h and d_r, we need to set $\left[\partial\bar{R}_1/\partial d_h\right] = 0$, $\left[\partial\bar{R}_1/\partial d_r\right] = 0$ and $\left[\partial\bar{R}_2/\partial d_h\right] = 0$, $\left[\partial\bar{R}_2/\partial d_r\right] = 0$. A closed-form solution does not exist, however it can be solved numerically by changing the values of d_h and d_r from zero to the constraint given by $\sqrt{d_h^2 + d_r^2} \leq d_{SD}$. Since the channel will be categorized as non-degraded channel otherwise and, according to earlier discussions in Section 4.4, relay should not be involved in the transmission. When optimized $\bar{R}_1$ and

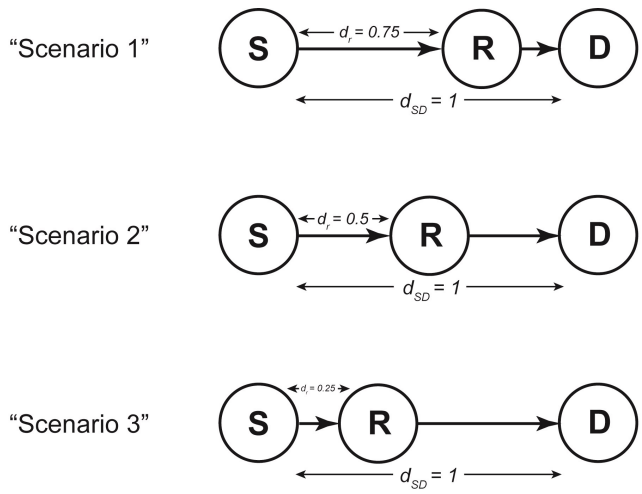

Figure 21: Representative scenarios.

$\bar{R}_2$ are found, we pick up the minimum one (recall the definition $\bar{R} = \min\left\{\bar{R}_1, \bar{R}_2\right\}$) and the corresponding values of d_h and d_r determine the optimum values of relay location.

4.5 Numerical Results

In this section, we present numerical results for the derived expressions within this chapter. Unless otherwise noted, we have the following assumptions: We consider a carrier frequency of 30 kHz and a transmission distance of $d = 1$ km. We assume temperature $T = 22°$C, depth $D = 50$ m, acidity of 8 pH, salinity $S = 35$ ppt, wind speed $\omega = 0$ m/s and spreading factor $s = 1.5$. We assume that the UWA channel experiences a multipath delay spread of 13 ms and has the order of $L = 130$. The number of significant delay taps is $m = 10$ and located at equal distances from each other with a uniform PDP, i.e. the power of each significant tap is $1/m$. The Rician k factor for the significant taps is 2 dB.

As examples, we consider three representative scenarios (see Fig. 21)

1) Scenario 1: $d_h = 0$ and $d_r = 0.75$

2) Scenario 2: $d_h = 0$ and $d_r = 0.5$

3) Scenario 3: $d_h = 0$ and $d_r = 0.25$

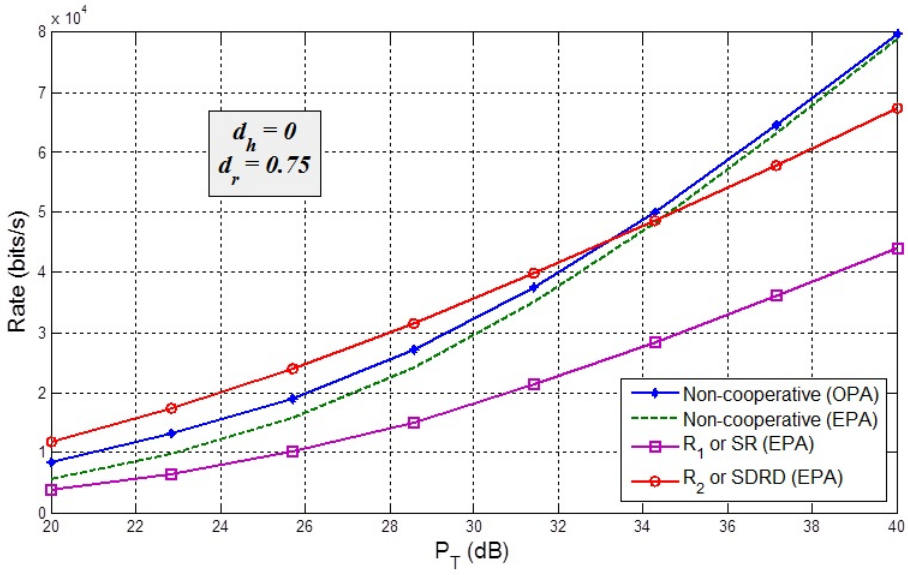

Figure 22: Rate versus total transmit power for $d_h = 0$ and $d_r = 0.75$.

In Fig. 22, the achiveable rates versus P_T are depicted for Scenario 1 where the relay is closer to destination. As benchmarks, we include the achievable rate of of a point-to-point non-cooperative channel (i.e., without the help of relay) assuming both optimal power allocation (OPA) and equal power allocation (EPA). These are illustrated respectively by the blue and green curves. The other two curves show the derived bounds on the achievable rates in relay-assisted case, c.f., $\bar{R}_1$ in (94) and $\bar{R}_2$ in (109). We observe that the minimum of $\bar{R}_1$ (violet) and $\bar{R}_2$ (red) curves is equivalent to $\bar{R}_1$ (violet) and is worse than the rate achievable by point-to-point link for all P_T values. The reason is that the relay is far enough from the source and has a very poor channel quality particularly because UWA channels suffer from significant attenuation as a function of distance. So if the source-to-relay channel is not sufficiently better than point-to-point link, it will limit the achievable rate and there would be waste of capacity in such scenarios when EPA is used. In this case, which is categorized as non-degraded channels (c.f. Section 4.4), the OPA performance (not shown in the figure) is equivalent to not involving the relay in the transmission and optimizing the point-to-point link which results the same as in the blue curve.

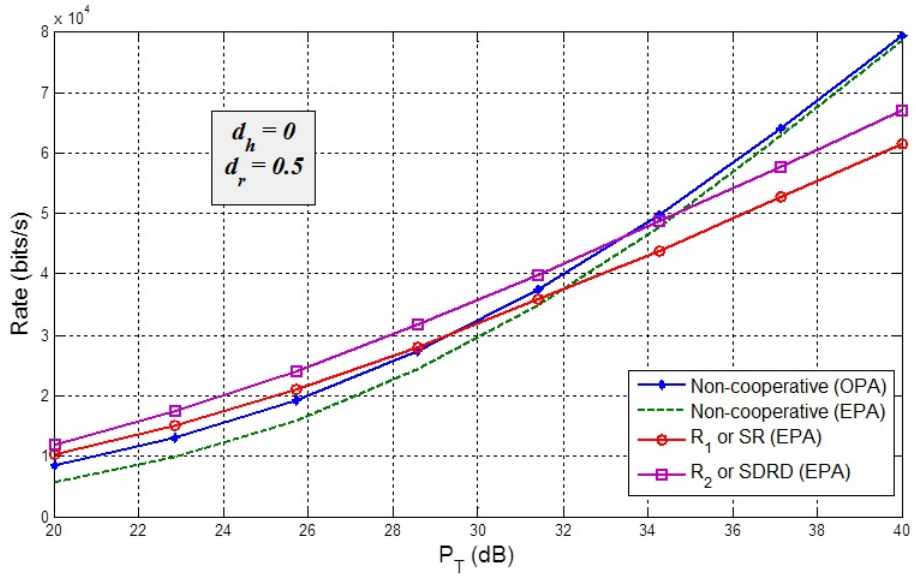

Figure 23: Rate versus total transmit power for $d_h = 0$ and $d_r = 0.5$.

In Fig. 23, the achievable rates versus P_T are depicted for Scenario 2 where the relay is in the middle of the path from source to destination. It is observed that the minimum of $\bar{R}_1$ (red) and $\bar{R}_2$ (violet) curves is equivalent to $\bar{R}_1$ (red). This indicates that source-to-relay channel will limit the rate. For low SNR values, the performance of relay channel is better and such cases are categorized as degraded channel. For low SNR values, the OPA performance (not shown in the figure) yields the same performance as violet curve ($\bar{R}_2$). But for high SNR values, the channel will be categorized as non-degraded and since the source-to-destination channel has a good quality itself, using the relay comes with some waste of capacity. The OPA for high SNR values results in the same performance as OPA of non-cooperative scenario (blue curve).

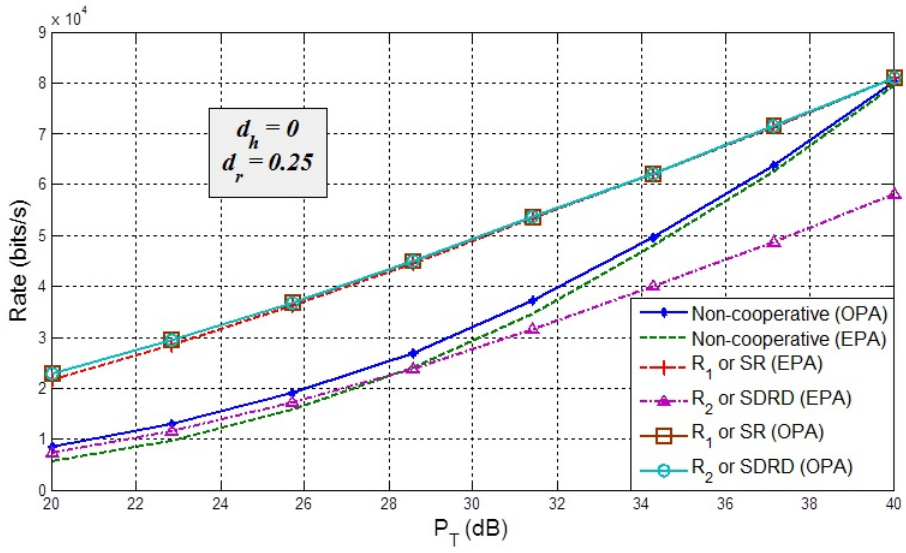

Figure 24: Rate versus total transmit power for $d_h = 0$ and $d_r = 0.25$.

In Fig. 24, the rates versus P_T are depicted for Scenario 3 where the relay is closer to the source terminal. It is observed that the minimum of $\bar{R}_1$ (red) and $\bar{R}_2$ (violet) curves is equivalent to $\bar{R}_2$ (violet). Since the relay is closer to source, it has better channel quality and will not limit the rate (degraded channel). It has been discussed in Section IV. d. that the achievable rate is optimized when the limitation bounds on the rate are equal. The more improvement here occurs in the second limitation bound on the rate, i.e. $\bar{R}_2$, which limits the achievable rate in EPA case. By optimized power allocation strategy, the point-to-point case can be outperformed even in high SNR cases.

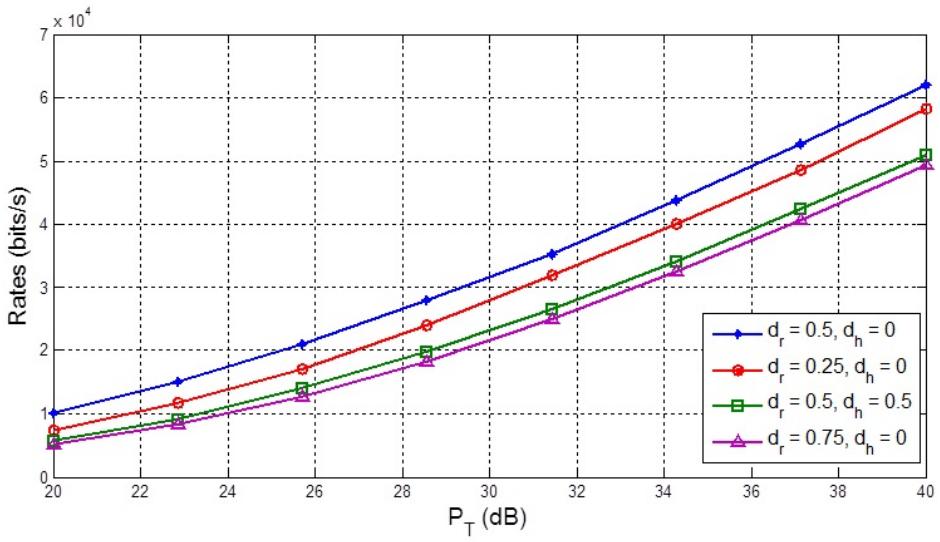

Figure 25: Rate versus total transmit power for different locations of relay (EPA is assumed).

In Fig. 25, we investigate the effect of different relay locations under the assumption of EPA. We observe that the optimized relay location is in the middle of the straight line connecting the source and the destination path. This is denoted by $d_r = 0.5$ and $d_h = 0$ (or equivalently by $d_{SR} = 0.5$ and $d_{RD} = 0.5$). We further observe that when the relay is more close to the source ($d_r = 0.25$, $d_h = 0$) , it has better performance in comparison to the case when the relay is closer to the destination node ($d_r = 0.75$, $d_h = 0$).

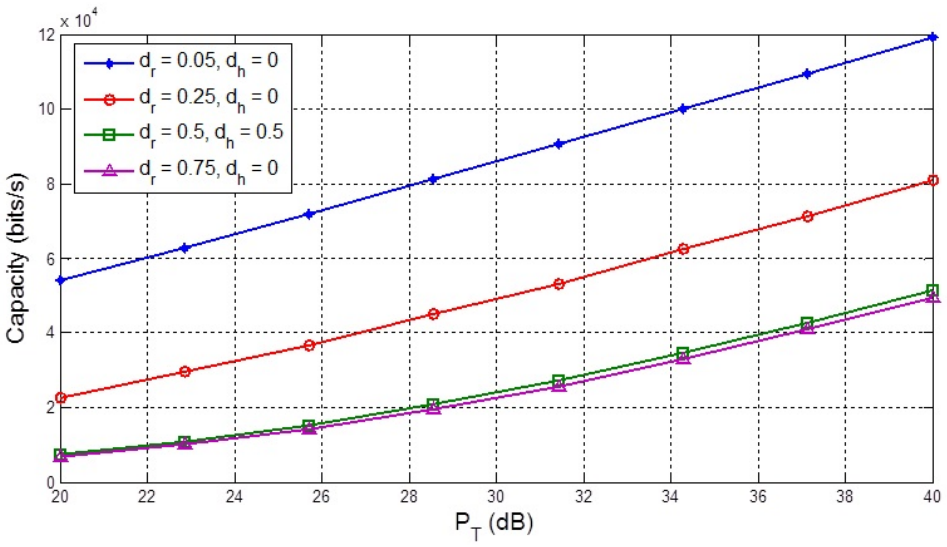

Figure 26: Rate versus total transmit power for different locations of relay (OPA is assumed).

In Fig. 26, we investigate the effect of different relay locations under the assumption of OPA. We observe that the optimized relay location for OPA case is when the relay is as much as possible close to source. The reason is that when the relay is very close to the source node, it will need less power for transmission to the relay node and more power is saved for the source and relay terminals to transmit with full power (i.e. P_T) to destination node. Hence, the hypothetical case of $d_r = 0$ and $d_h = 0$ should yield the best performance. Following the fact that optimal cooperative case happens when source and relay nodes are at the same place and transmit with full power of P_T to destination, it may be questioned that what is the advantage of relay assisted case over a point-to-point scenario with transmit power of $2P_T$? This point-to-point scenario does not follow the power constraint, however, in cooperative case we are using the benefits of relay node and it does not exceed the power constraint and outperform the point-to-point case with transmit power of P_T.

CHAPTER V

CONCLUSION

In this thesis, we have worked on the information theoretical performance analysis and optimization of point-to-point and relay-assisted UWA systems. We have assumed a single-carrier communication architecture and sparse Rician frequency-selective UWA channel with ISI. We have considered non-white Gaussian distribution to model the ambient noise and taken into account the effects of environmental parameters such as temperature, salinity, pressure as well as distance and frequency.

In the first part of the thesis, we have developed an equivalent channel model for UWA channel with ISI under consideration and shown that the capacity of the equivalent channel converges to that of the operating channel in the limit of infinite block length. Using these results, we have first obtained a capacity expression for the UWA channel and demonstrated the dependency on channel parameters such as the number and location of significant taps and power delay profile, and environmental parameters such as temperature, salinity, and pressure. Then, we have used this expression to determine the optimal carrier frequency, input signaling, and bandwidth.

In the second part of the thesis, we have extended our results to cooperative UWA systems and obtained achievable rates of single-carrier cooperative UWA systems with orthogonal DF relaying. Specifically, we have derived the achievable rates taking into account the effect of relay geometry and determined the achievable maximum rates by optimal input signaling. We have further determined the location of the relay to optimize the achievable rates. Our results have demonstrated that optimized relay location in EPA case is in the middle of the straight line connecting the source and the destination. On the other hand, for OPA case, we observe that the relay should be located as much as possible close to source to optimize the performance.

APPENDIX A

DERIVATION OF OPTIMAL CARRIER FREQUENCY

In order to derive the optimal frequency, we begin with (51). For $10 \leq f \leq 100$ kHz, we can approximate $\partial Z_w(f)_{\text{dB}}/\partial f$ by

$$\frac{\partial Z_w(f)_{\text{dB}}}{\partial f} \cong \frac{-20}{\ln(10)} \frac{1}{f}. \tag{122}$$

Recall that $a(f)_{\text{dB}}$ is given by (2). Let us define $M_1 = (A_1 B_1 C_1 f^2) / (C_1^2 + f^2)$, $M_2 = (A_2 B_2 C_2 f^2) / (C_2^2 + f^2)$, $M_3 = A_3 B_3 f^2$. In the frequency range under consideration, we can safely assume $M_1 \cong 0$, $M_3 \cong 0$, since M_2 (involving $MgSO_4$ contributions) dominates the others [25]. Therefore, we have

$$\frac{\partial a(f)_{\text{dB}}}{\partial f} \cong \frac{2A_2 B_2 {C_2}^3 f}{\left({C_2}^2 + f^2\right)^4}. \tag{123}$$

Replacing (122) and (123) in (51) and defining $\alpha = 10/d \ln(10)$, we obtain

$$\alpha f^4 + \left(2\alpha {C_2}^2 - A_2 B_2 {C_2}^3\right) f^2 + \alpha {C_2}^4 = 0 \tag{124}$$

which is a quadratic equation. Within $10 \leq f \leq 100$ kHz and under the assumptions of $-2^\circ \leq T \leq 22^\circ$, $S = 30 - 35$ppt, and $D \leq 3.5$ km [25], we have $C_2^4 \gg f^4$. Therefore, we can approximate (124) by $\left(2\alpha {C_2}^2 - A_2 B_2 {C_2}^3\right) f^2 + \alpha {C_2}^4 = 0$ where the approximated solution is given by

$$f = C_2 \sqrt{\frac{\alpha}{A_2 B_2 C_2 - 2\alpha}}. \tag{125}$$

Noting $A_2 B_2 = 0.52\,(1 + T/43)\,(S/35)\,e^{-D/6}$ and $C_2 = f_2 = 42e^{(T/17)}$ [37], the optimal frequency can be found as

$$f \cong \sqrt{\frac{367.5}{\frac{S}{35}\left(1 + \frac{T}{43}\right) \exp\left(-\frac{D}{6} - \frac{T}{17}\right) d - 0.28 \exp\left(-\frac{2T}{17}\right)}}. \tag{126}$$

APPENDIX B

OPTIMAL BANDWIDTH DERIVATIONS FOR SINGLE REALIZATION OF UWA CHANNEL

In this appendix, we optimize the capacity with respect to bandwidth for one realization of UWA channel. First note that the instantaneous capacity is given by (28)

$$C = \max_{W} \frac{1}{2} \int_{W} \log\left(1 + \frac{P(f)}{\beta(f)}\right) df$$
$$\text{subject to} \int_{W} P(f) df \leq E_s \tag{127}$$

where $\beta(f) = Z_w(f)/G(f,d)$. In the following, we will consider two cases.

No CSI at transmitter: Under the assumption that CSI is only present at the receiver side, we can simply use equal power allocation. Simply replacing $P(f) = E_s/W$ in (127) and differentiating the resulting expression with respect to W and setting it to zero, we have

$$\frac{dC(W)}{dW} = \frac{d\left[\frac{1}{2}\int_{f_c-W/2}^{f_c+W/2} \log_2\left(1 + \frac{E_s/W}{\beta(f)}\right) df\right]}{dW} = 0. \tag{128}$$

Here, we use the *Leibnitz Rule*, i.e.

$$g(x) = \int_{a(x)}^{b(x)} f(x,t)\, dt \;\rightarrow\; \frac{dg}{dx} = \frac{db}{dx} f(x, b(x)) - \frac{da}{dx} f(x, a(x)) + \int_{a(x)}^{b(x)} \frac{\partial f(x,t)}{\partial x} dt \tag{129}$$

to solve (128), i.e.,

$$\frac{1}{2}\log_2\left(1 + \frac{E_s/W}{\beta(f_c + W/2)}\right) + \frac{1}{2}\log_2\left(1 + \frac{E_s/W}{\beta(f_c - W/2)}\right) = \frac{1}{W \ln 2} \int_{f_c-W/2}^{f_c+W/2} \left(1 + \frac{\beta(f)}{E_s/W}\right)^{-1} df. \tag{130}$$

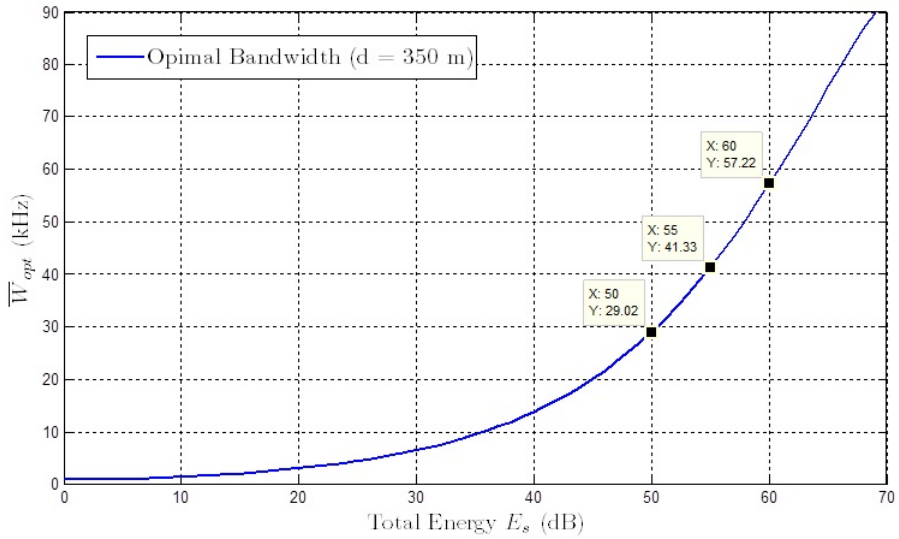

Figure 27: Averaged optimal bandwidth vs. total energy of input signal.

By some manipulations, we have

$$\ln\left(1+\frac{E_s/W}{\beta\left(f_c+W/2\right)}\right)+\ln\left(1+\frac{E_s/W}{\beta\left(f_c-W/2\right)}\right)=\frac{2}{W}\int_{f_c-W/2}^{f_c+W/2}\left(1+\frac{\beta\left(f\right)}{E_s/W}\right)^{-1}df \quad (131)$$

from which the optimal bandwidth is solved. Then we average the optimal bandwidths for all realizations of the channel.

In Fig. 27, we assume $T = 22°\text{C}$, $D = 50$ m, $S = 35$ ppt, $d = 350$ m, and $f_{opt} = 55$ kHz. In this figure we depict average of optimal bandwiths for different values of E_s. From this figure, we observe that the averaged optimal bandwidths of 29.02, 41.33, 57.22 kHz are achieved respectively for for $E_s = 50$, 55, and 60 dB.

CSI available at the transmitter: Assuming CSI is present at the transmitter, we can perform waterfilling to *simultaneously* optimize the PSD and bandwidth. Specifially, assuming a fixed E_s, optimal bandwidth can be found as the range of frequencies between $f_{1,\text{opt}}$ and $f_{2,\text{opt}}$. These are the solutions to the equation $\beta\left(f\right) = v$ where v is solved from

$$\int_{\beta_1^{-1}(v)}^{\beta_2^{-1}(v)}\left[v-\beta\left(f\right)\right]^{+}df=E_s. \quad (132)$$

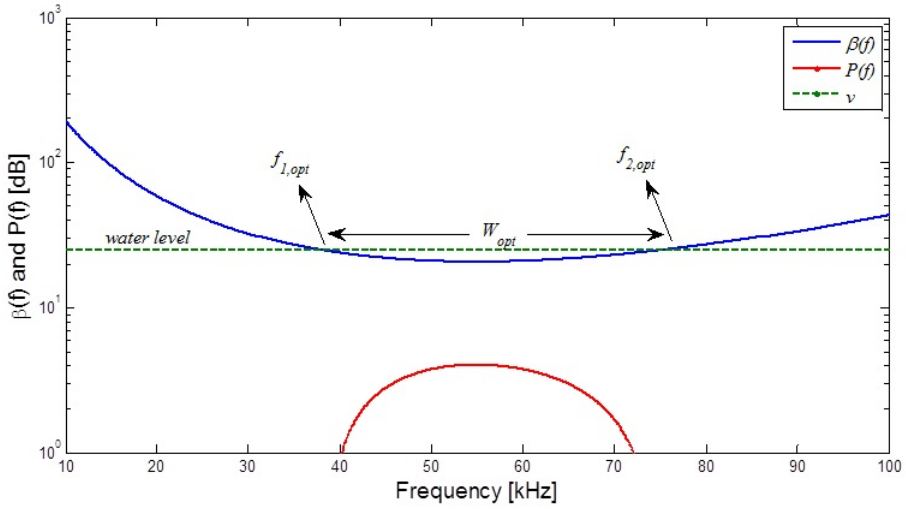

Figure 28: Optimal bandwidth and water level for $E_s = 50$ dB.

Therefore, the optimal bandwidth is given by $W_{\text{opt}} = f_{2,\text{opt}} - f_{1,\text{opt}}$ where $f_{1,\text{opt}} = \beta_1^{-1}(v)$, $f_{2,\text{opt}} = \beta_2^{-1}(v)$.

In Fig. 28, we assume $T = 22°\text{C}$, $D = 50$ m, $S = 35$ ppt, $d = 350$ m, and $f_{opt} = 55$ kHz and for a single realization of the channel the optimal bandwidth is depicted. By numerical results, the optimal bandwidths for this scenario are equaivalent to the first scenario, since input signalling, $P(f)$, do not participate in bandwidth optimization. In the first scenario, equal power is allocated and optimal bandwidhs are found, while in this scenario, capacity is optimized through optimal signalling and optimal bandwidths are found.

Bibliography

[1] F. Fahy and J. Walker, *Fundamentals of Noise and Vibration*. Taylor & Francis, 2003.

[2] R. J. Urick, *Principles of Underwater Sound*. 3rd Edition. New York: McGraw-Hill, 1983.

[3] M. Stojanovic, J. A. Catipovic, and J. G. Proakis, "Phase-coherent digital communications for underwater acoustic channels," *IEEE J. of Oceanic Eng.*, vol. 19, no. 1, pp. 100–111, Jan. 1994.

[4] W. Li and J. C. Preisig, "Estimation of rapidly time-varying sparse channels," *IEEE J. of Oceanic Eng.*, vol. 32, no. 4, pp. 927–939, Oct. 2007.

[5] M. Stojanovic, L. Freitag, and M. Johnson, "Channel-estimation-based adaptive equalization of underwater acoustic signals," in *OCEANS'99 MTS/IEEE*, vol. 2, pp. 590–595, 1999.

[6] A. A. Rontogiannis and K. Berberidis, "Bandwidth efficient transmission through sparse channels using a parametric channel-estimation-based DFE," *IEEE Proc. Communications*, vol. 152, no. 2, pp. 251–256, 2005.

[7] Y. F. Cheng and D. M. Etter, "Analysis of an adaptive technique for modeling sparse systems," *IEEE Trans. on Acoustics Speech and Signal Processing*, vol. 37, no. 2, pp. 254–264, Feb. 1989.

[8] B. Li, J. Huang, S. Zhou, K. Ball, M. Stojanovic, L. Freitag, and P. Willett, "MIMO-OFDM for high-rate underwater acoustic communications," *IEEE J. of Oceanic Eng.*, vol. 34, no. 4, pp. 634–644, Oct. 2009.

[9] Y. Emre, V. Kandasamy, T. M. Duman, P. Hursky, and S. Roy, "Multi-input multi-output OFDM for shallow-water UWA communications," *Journal of the Acoustical Society of America*, vol. 123, no. 5, 2008.

[10] B. Li, S. Zhou, M. Stojanovic, L. Freitag, and P. Willett, "Multicarrier communication over underwater acoustic channels with nonuniform doppler shifts," *IEEE J. of Oceanic Eng.*, vol. 33, no. 2, pp. 198–209, Apr. 2008.

[11] S. Roy, T. M. Duman, V. McDonald, and J. G. Proakis, "High-rate communication for underwater acoustic channels using multiple transmitters and space–time coding: Receiver structures and experimental results," *IEEE J. of Oceanic Eng.*, vol. 32, no. 3, pp. 663–688, Jul. 2007.

[12] A. Song, M. Badiey, and V. K. McDonald, "Multichannel combining and equalization for underwater acoustic MIMO channels," *in Proc. MTS/IEEE OCEANS Conf.*, Quebec City, Canada, Sep. 2008.

[13] J. Tao, Y. R. Zheng, C. Xiao, T. Yang, and W. B. Yang, "Time-domain receiver design for MIMO underwater acoustic communications," *in Proc. MTS/IEEE OCEANS Conf.*, Quebec City, Canada, Sep. 2008.

[14] J. Zhang, Y. Zheng, and C. Xiao, "Frequency-domain equalization for single carrier MIMO underwater acoustic communications," *in Proc. MTS/IEEE OCEANS Conf.*, Quebec City, Canada, Sep. 2008.

[15] C. Carbonelli, S. H. Chen, and U. Mitra, "Error propagation analysis for underwater cooperative multi-hop communications," *Elsevier J. Ad Hoc Networks*, vol. 7, no. 4, pp. 759–769, June 2009.

[16] W. Zhang, M. Stojanovic, and U. Mitra, "Analysis of a linear multihop underwater acoustic network," *IEEE J. of Oceanic Eng.*, vol. 35, no. 4, pp. 961–970, Oct. 2010.

[17] S. Al-Dharrab, M. Uysal, and T. Duman, "Cooperative underwater acoustic communications," *IEEE Communications Magazine*, vol. 51, no. 7, Jul. 2013.

[18] L. M. Brekhovskikh and Y. P. Lysanov, *Fundamentals of Ocean Acoustics*. New York: Springer, 2003.

[19] M. Stojanovic, "On the relationship between capacity and distance in an underwater acoustic communication channel," *ACM SIGMOBILE Mobile Computing and Comm. Rev.*, vol. 11, no. 4, pp. 34–43, 2007.

[20] C. Choudhuri and U. Mitra, "Capacity bounds and power allocation for underwater acoustic relay channels with ISI," *Proceedings of the Fourth ACM International Workshop on UnderWater Networks*, p. 6, 2009.

[21] C. Polprasert, J. A. Ritcey, and M. Stojanovic, "Capacity of OFDM systems over fading underwater acoustic channels," *IEEE J. of Oceanic Eng.*, vol. 36, no. 4, pp. 514–524, Oct. 2011.

[22] H. Kwon and T. Birdsall, "Channel capacity in bits per joule," *IEEE J. of Oceanic Eng.*, vol. 11, no. 1, pp. 97–99, Jan. 1986.

[23] H. A. Leinhos, "Capacity calculations for rapidly fading communications channels," *IEEE J. of Oceanic Eng.*, vol. 21, no. 2, pp. 137–142, 1996.

[24] R. Coates, *Underwater Acoustic Systems*. Hong Kong: Macmillan, 1990.

[25] R. Francois and G. Garrison, "Sound absorption based on ocean measurements: Part I: Pure water and magnesium sulfate contributions," *The Journal of the Acoustical Society of America*, vol. 72, p. 896, 1982.

[26] R. Francois and G. Garrison, "Sound absorption based on ocean measurements. Part II: Boric acid contribution and equation for total absorption," *The Journal of the Acoustical Society of America*, vol. 72, no. 6, pp. 1879–1890, 1982.

[27] W. Hirt and J. Massey, "Capacity of the discrete-time Gaussian channel with intersymbol interference," *IEEE Trans. on Info. Theory*, vol. 34, no. 3, pp. 38–38, 1988.

[28] J. Proakis, *Digital Communications*. McGraw-Hill, 1995.

[29] A.Radosevic, J.Proakis, and M.Stojanovic, "Statistical characterization and capacity of shallow water acoustic channels," *IEEE Oceans Europe Conf.*, pp. 1–8, 2009.

[30] A. Goldsmith and M. Effros, "The capacity region of broadcast channels with intersymbol interference and colored Gaussian noise," *IEEE Trans. on Info. Theory*, vol. 47, no. 1, pp. 219–240, 2001.

[31] T. M. Cover and J. A. Thomas, *Elements of Information Theory*. Wiley-interscience, 2006.

[32] M. K. Simon and M. S. Alouini, *Digital communication over fading channels*. Wiley, 2005.

[33] W. C. Lee, "Estimate of channel capacity in rayleigh fading environment," *IEEE Transactions on Vehicular Technology*, vol. 39, no. 3, pp. 187–189, Aug. 1990.

[34] H. W. Chen and K. Yanagi, "The convex-concave characteristics of gaussian channel capacity functions," *IEEE Trans. on Info. Theory*, vol. 52, no. 5, pp. 2167–2172, May 2006.

[35] J. N. Laneman, D. N. Tse, and G. W. Wornell, "Cooperative diversity in wireless networks: Efficient protocols and outage behavior," *IEEE Trans. on Info. Theory*, vol. 50, no. 12, pp. 3062–3080, Dec. 2004.

[36] B. Suard, G. Xu, H. Liu, and T. Kailath, "Uplink channel capacity of space-division-multiple-access schemes," *IEEE Trans. on Info. Theory*, vol. 44, no. 4, pp. 1468–1476, Jul. 1998.

[37] M. A. Ainslie and J. G. McColm, "A simplified formula for viscous and chemical absorption in sea water," *Journal of the Acoustical Society of America*, vol. 103, no. 3, pp. 1671–1672, 1998.

VITA

Hatef Nouri was born in Tehran, Iran, 1988. He is currently pursuing M.Sc. degree in Electrical and Electronics Engineering at Özyeğin University, Istanbul, Turkey. He is member of CT&T Research Group headed by Prof. Murat Uysal. Hatef received his B.Sc. degree in electrical engineering from University of Tehran, Tehran, Iran, in 2010. His research interests are in Information Theory, Wireless Communications, Underwater Acoustic Communication, Free Space Optic, Digital Communication Systems and Coding.